EFFECTS OF MOLYBDENUM NANOPARTICLES ON THE INTERFACE BETWEEN LEAD-FREE SOLDER AND NICKEL SUBSTRATE

MOHAMMAD HOSSEIN MAHDAVIFARD

RESEARCH PROJECT SUBMITTED IN PARTIAL
FULFILMENT OF THE REQUIREMENTS FOR THE
DEGREE OF MASTER OF ENGINEERING

FACULTY OF ENGINEERING
UNIVERSITY OF MALAYA
KUALA LUMPUR

2013

UNIVERSITY OF MALAYA

ORIGINAL LITERARY WORK DECLARATION

(I.C/Passport No: **U19765890**) Registration/Matric No:

Name of Candidate: **Mohammad Hossein Mahdavifard**

Name of Degree: **MASTER OF MATERIALAS ENGINEERING AND TECH**

Title of Project Paper/Research Report/Dissertation/Thesis (“this Work”):

Effect of Molybdenum nanoparticles on lead free solders on copper substrate with Nickel layer

Field of Study: **Materials Engineering**

I do solemnly and sincerely declare that:

1) I am the sole author/writer of this Work;
2) This Work is original;
3) Any use of any work in which copyright exists was done by way of fair dealing and for permitted purposes and any excerpt or extract from, or reference to or reproduction of any copyright work has been disclosed expressly and sufficiently and the title of the Work and its authorship have been acknowledged in this Work;
4) I do not have any actual knowledge nor do I ought reasonably to know that the making of this work constitutes an infringement of any copyright work;
5) I hereby assign all and every rights in the copyright to this Work to the University of Malaya (“UM”), who henceforth shall be owner of the copyright in this Work and that any reproduction or use in any form or by any means whatsoever is prohibited without the written consent of UM having been first had and obtained;
6) I am fully aware that if in the course of making this Work I have infringed any copyright whether intentionally or otherwise, I may be subject to legal action or any other action as may be determined by UM.

Candidate’s Signature Date

Subscribed and solemnly declared before,

Witness’s Signature Date

Name:

Designation:

Abstract

In this study, Mo nanoparticles were used as a reinforcing material into the Sn-3.8Ag-0.7Cu (SAC) solder on the nickel substrate (Cu substrate with an electrodeposited Ni layer on top). The Mo nanoparticles were characterized by transmission electron microscopy (TEM) and X-ray diffractometer (XRD). The composite solder paste was prepared by manually mixing Mo nanoparticles with the SAC solder paste. Nickel was electrodeposited on polycrystalline copper substrate in the Watts bath. The solder paste was placed on substrate at 250ºC for 45 seconds. After reflow, elemental compositions of the nanocomposite solders were analyzed by inductively coupled plasma-optical emission spectrometer (ICP-OES). The microstructural investigations, spreading rate and wetting angle measurement were carried out on the solders after first reflow. After that one set of samples were subjected to multiple reflow for up to six times. Microstructural investigations were performed at the solder/substrate interface using high resolution field emission scanning electron microscopy (FESEM) and energy dispersive X-ray (EDX). Results reveal that after reflow only a fraction of Mo nanoparticles were retained inside the solder matrix. The solder spreading rate was decreased and wetting angle increased with the addition of Mo nanoparticles to the SAC solder. It was found that Mo nanoparticles were effective in suppressing the growth of total IMC layer thickness and scallop diameter during reflow. It was found that Mo nanoparticles did not dissolve or react with the solder during reflow. The retardation of IMC thickness was suggested to be due to the discrete particle effect of Mo nanoparticles. The intact, discrete nanoparticles, by absorbing preferentially at the interface, hindered the diffusion flux of the substrate and thereby suppressed the IMC growth. The retardation of total IMC layer with the addition of Mo nanoparticles is expected to improve the reliability of the solder joint.

Abstrak

Dalam kajian ini, nanopartikel Mo telah digunakan sebagai bahan pengukuh dalam Sn-3.8Ag-0.7Cu (MPS) pateri pada substrat Nickel (substrat Cu dengan electrodeposited Ni lapisan). Nanopartikel Mo telah disifatkan oleh penghantaran elektron mikroskop (TEM) dan sinar-X diffractometer (XRD). Pes pateri komposit telah disediakan secara manual dengan pencampuran nanopartikel Mo ke dalam pes pateri SAC. Nikel telah electrodeposited pada polihabluran tembaga substrat dengan kaedah mandi watt. Pes pateri diletakkan pada substrat apabila suhu mencapai 250 º C selama 45 saat. Selepas reflow, komposisi unsur yang solders Komposit nano akan dianalisis oleh induktif yang ditambah dengan spektrometer pelepasan plasma-optik (ICP-OES). Siasatan mikrostruktur, kadar merebak dan sudut pembasahan telah dijalankan pada solders selepas reflow pertama. Selepas itu, set sampel tersebut akan diuji dalam reflow selama enam kali. Mikrostruktur siasatan akan dijalankan di antara permukaan pateri / substrat dengan menggunakan bidang pelepasan imbasan mikroskop elektron (FESEM) yang resolusi tinggi dan serakan tenaga sinar-X (EDX). Keputusan dari ujian menunjukkan bahawa selepas reflow, hanya sebahagian kecil daripada nanopartikel Mo telah mengekalkan dalam matriks pateri. Kadar menyebarkan telah menurun dan sudut membasahkan meningkat dengan tambahan nanopartikel Mo dalam pateri MPS. Ia didapati bahawa nanopartikel Mo berkesan dalam membenteras pertumbuhan jumlah ketebalan lapisan IMC dan diameter kerang semasa reflow. Dengan tambahan nanopartikel Mo, pekali penyebaran dikurangkan tetapi tenaga pengaktifan pertumbuhan kerang IMC masih tidak berubah. Pembubaran substrat Cu dan pembentukan IMC dikurangkan dengan kehadiran nanopartikel Mo.
Dari keputusan penyelidikan, ia telah mendapati bahawa nanopartikel Mo tidak larut atau bertindak-balas dengan pateri semasa reflow. Ketebalan IMC dan diameter kerang

terencat adalah disebabkan oleh kesan zarah diskret nanopartikel Mo. Tindak-balas, nanopartikel diskret, dengan menyerap terutamanya pada permukaan, menghalang fluks penyebaran substrat dan pertumbuhan IMC itu. Jumlah lapisan IMC yang terencat dengan tambahan nanopartikel Mo meningkatkan kebolehpercayaan sendi pateri.

Acknowledgements

First, I would like to express my deep and sincere gratitude to my supervisor, Prof. Dr. A.S. Md. Abdul Haseeb for his technical advices and constructive comments throughout this dissertation.

I would like to sincere thanks to my dear friends and colleagues. Many thanks to Md. Arafat Mahmood for his useful comments that improved the dissertation. Special thanks to Hamid Taheri for being a very helpful friend.

Finally, the people close to my heart deserve the uppermost appreciation for their support and patience. Many special thanks to my dear parents and my dear sister. I always feel the warmth of their love.

Table of Contents

List of Figures

List of Tables

List of Notations

SAC = Sn-3.8Ag-0.7Cu

Sn = Tin

Ag = Silver

Cu = Copper

Pb = Lead

Mo = Molybdenum

Co = Cobalt

Ni = Nickel

Au = Gold

Bi = Bismuth

Zn = Zinc

In = Indium

IMC = Intermetallic compound

H_2SO_4 = Sulphuric acid

HNO_3 = Nitric acid

HCl = Hydrochloric acid

CNT = Carbon nanotube

TiO_2 = Titanium dioxide

Al_2O_3 = Alumina

nm = Nanometer

μm = Micrometer

List of Abbreviation

TEM = Transmission Electron Microscopy

SEM = Scanning Electron Microscopy

FESEM = Field Emission Scanning Electron Microscopy

EDX = Energy Dispersive X-Ray

XRD = X-ray Diffraction

DSC = Differential Scanning Calorimeter

ICP-OES = Inductive Couple Plasma- Optical Emission Spectrometer

ITRS = International Technology Roadmap for Semiconductor

EPA-US = Environmental Protective Agency-United States

NCMS = National Center for Manufacturing Science

EU = European Union

WEEE = Waste Electrical and Electronic Equipment

IC = Integrated Circuit

PCB = Printed Circuit Board

BGA = ball Grid Array

FC = Flip Chip

SMT = Surface Mount Technology

PIH = Pin in Hole

PTH = Pin through Hole

OSP=Organic Solderability Preservative

NEMI= National Electronics Manufacturing Initiative

RoHS= Restriction of hazardous substance Directives

Chapter 1: Introduction

1.1 Background

Soldering is one of the important famous joining methods that use a filler metal with a melting point below 425°C. In the immense electronic materials world, solder plays a vital role in the assembly and interconnection of the silicon die (or chip). As a joining material, solder provides electrical, thermal and mechanical continuity in electronics assemblies. The performance and quality of the solder are crucial to the integrity of a solder joint, which in turn is vital to the overall functioning of the assembly (Abtew and Selvaduray, 2000).

The primary solder alloy design criteria have been developed by using Sn-Pb eutectic as a baseline. For more than fifty years, printed wiring boards (PWB) and components had been designed around the behavior of Sn-Pb eutectic solder during circuit board assembly and in use for holding components to the PWBs (Bath, 2010). As a result of toxicity of Pb, the new standard Pb-free alloy replaces Sn-Pb eutectic solder in a wide variety of board designs and microelectronics applications.

The Waste Electrical and Electronic Equipment (WEEE) Directive encourages increased recycling of electrical and electronic products. However, the recycling effort is typically an end-of-use action that occurs just prior to potential disposal. As a purely environmental strategy, Pb elimination/replacement appears to be a better approach, unless the substitutions cause more problems than they solve (Ganesan and Pecht, 2006).

By 1999, the WEEE and Restriction of Hazardous Substance Directives (RoHS) led National Electronics Manufacturing Initiative (NEMI) to establish a less quantitative, but no less restrictive, set of criteria. The NEMI alloy was designed to:

1. Have a melting point as close as possible to Sn-Pb eutectic

2. Be eutectic or very close to eutectic alloy
3. Contain maximum three elements (ternary composition)
4. Avoid using existing patents (avoid legal obligation)
5. Have the potential for reliability equal to or better than Sn-Pb eutectic solder (Bath, 2010).

All research groups agreed that there were no “drop-in” replacement alloys for Sn-Pb eutectic. Applications of these criteria led the NEMI to choice the Sn-Ag-Cu ternary system, more specifically the Sn-3.9Ag-0.6Cu (± 0.2%) alloy that it has the most promising properties for surface mount application.

One of the major challenges in the development of a reliable Pb-free solder is to improve the mechanical, interfacial properties and reliability of the solder joints (Koo and Jung, 2005). The microstructure of SAC alloys has been found to coarsen to a greater extent during use and during high temperature exposure as compared with that of their Pb containing counterparts (Cheng et al., 2009). Moreover, Sn based solders form thicker intermetallic compound (IMC) layer at the solder/substrate interface compared with the Pb based solders (Wu et al., 2004). The interfacial IMCs in Pb-free solder also grow at a faster rate than that in Pb-based solders. Coarsening of microstructure and rapid growth of brittle interfacial IMC are known to degrade the properties of lead free solder joints resulting in lower long term reliability.

Adding appropriate additions to Sn based solder is one approach to improve its properties. Alloy addition (Wang et al., 2008b) and particle additions (Das et al., 2009, Shen and Chan, 2009) has been studied recently. Adding particles to Sn based solder results in the development of composite solders with superior properties. Addition of diverse types and sizes of particles are under investigations. Many kinds of particles that have been investigated until now include metallic (Amagai, 2008, Lin et al., 2002), ceramics (Shen and Chan, 2009) and carbon nanotubes (Kumar, 2009) . Both micrometer (Das et al., 2009) and nanometer (Shi et al., 2008) sized particles are currently being considered.

The reason behind particle addition is that by adding appropriate types of particles to the solder, they should lead to dispersion strengthening. They are also anticipated to stabilize the microstructure by limiting the growth of different phases in the solder during use. Nanoparticles addition to tin based solders are attracted many consideration in recent years (Amagai, 2008). With the miniaturization of solder pitch size in electronic packages, the additions of nanoparticles are becoming more reliable method to reach the criteria of proper solder joint.

Improving in bulk mechanical properties like strength (Shen and Chan, 2009), hardness (Gain et al., 2011), creep resistance (Shi et al., 2008) etc. have been perceived in Pb-free solders reinforced by nanoparticles additions. Specifically, the addition of Mo nanoparticles has led in significant improvement in the bulk mechanical properties of solder (Chandra Rao et al., 2010, Kumar et al., 2005). Nevertheless, the integrity of a solder joint not only depends on its bulk properties, but also relies on the interfacial properties of the solder/substrate. Therefore, it is important to investigate the effect of the nanoparticles additions on the interfacial characteristics. Only a few studies are available on the influence of nanoparticles on the interfacial IMC.

1.2 Research Objectives

The objectives of this research are listed below:

1. To examine the wetting and reflow characteristics of Sn-3.8Ag-0.7Cu solder on Ni substrate with and without Mo nanoparticles.
2. To investigate the effects of Mo nanoparticles on the morphology and growth of intermetallic compounds during reflow on Ni substrate

3. To compare the effects of Ni substrate with Cu substrate in present of Mo nanoparticle on the morphology and growth of intermetallic compounds during reflow.

1.3 Scope of Research

The overall purpose of this research is to investigate the effect of molybdenum (Mo) nanoparticles on the interfacial reactions between Sn-3.8Ag-0.7Cu solder and Ni substrate, during multiple times of reflow. Therefore, Mo nanoparticles were manually mixed with the SAC solder paste at various wt% to prepare composite solder paste. A Ni layer was deposited on copper substrate and solder joints were prepared on the substrate under standard experimental conditions.

The characterizations of nanocomposite solder joints were carried out using several analytical methods. SAC solder joint was used as an experimental reference. All obtained data were compared and analyzed with other published works. The characterization of raw materials was carried out thoroughly by transmission electron microscopy (TEM), field emission scanning electron microscopy (FESEM) and X-ray diffraction (XRD) analysis. The melting behavior of the nanocomposite solders was investigated by differential scanning calorimeter (DSC). Inductively coupled plasma-optical emission spectrometry (ICP-OES) was utilized to find the actual amount of nanoparticles incorporated to the solder. The spreading rate and wetting angle of the solders were measured by the Japanese Industrial Standard (JIS Z3198-3, 2003). The interfacial microstructure following the solder samples were investigated by optical microscopy, conventional SEM, high resolution field emission SEM (FESEM) equipped with Energy Dispersive X-Ray (EDX).

1.4 Organization of Research Report

This research report consists of five chapters. Chapter 1 introduces briefly this research work. This chapter consist of the research background, the current technical problems in this field, research objectives and the scope of this research. Chapter 2 gives a general overview of the previous research on various topics related with this research. It includes electronic packaging and soldering technology, lead-free solder candidates, thermodynamics of alloy selection, interfacial reaction between the solder and substrate during reflow, Ni electroplating, effect of alloying elements and effects of nanoparticles on the solder. In Chapter 3, the experimental procedure is explained which consist of the procedures of sample preparations and electro-deposition, characterization techniques, the equipment, fixtures and procedure used during characterization. Chapter 4 reports the results from the experimental work and interpretation on the basis of analyze and comparison with the previous published document. Chapter 5 includes a brief summary of this research report and the recommendation for future work.

Chapter 2: Literature Review

2.1 Soldering technology and theirs metallurgy

Soldering involve using a molten filler metal to wet the mating surfaces of a joint, with or without the aid of a fluxing agent, leading to the formation of metallurgical bonds between the filler and the respective components. In these processes, the original surfaces of the components are “eroded” by virtue of the reaction occurring between the molten filler metal and the solid components. However the extent of this “erosion” is usually at the microscopic level (<100 µm) (Humpston and Jacobson, 2004).

Solder should have the following characteristic to be compatible with a particular parent material:

1. A liquidus temperature of the solder materials should be below the melting point (solidus temperature) of the parent materials and any surface metallizations.
2. Capability of producing joints at temperatures at which the properties of the base materials are not degraded.
3. The ability of the parent materials, or a metallization applied to the parent materials, to be wetted in order to ensure good adhesion through the formation of metallic bonds.
4. Limited erosion of the parent metals at the joint interface.
5. Elimination of constituents or impurities that might embrittle or otherwise weaken the resulting joint (Humpston and Jacobson, 2004).

Electronic packaging industries are depending on soldering technology at various levels for instance, wire bonding in surface mount technology, solder ball connection in ball grid arrays (BGA), IC package assembly in printed circuit board (PCB) or flip chip (FC) connections (Kang and Sarkhel, 1994). Solder joint provides the electrical connections between the component in combination of thermal, physical and mechanical support in the electronic devices (Abtew and Selvaduray, 2000). Solder joints should perform all of these functions; otherwise the reliability of the whole electronic system is threatened and may cause a failure of the package.

Reliability of solder joint technology in the microelectronic packaging industry has been a concern for a long time, such as, the low cycle fatigue of Sn-Pb solder joints in flip chip technology due to the cyclic thermal stress between a Si chip and its substrate. At present, the risk of fatigue has been much reduced by the innovative application of underfill of epoxy between the chip and its substrate. On the other hand, to replace Sn-Pb solders by Pb-free solders, new reliability issues have appeared, mostly because the Pb-free solders have a very high concentration of Sn. Furthermore, due to the demand of greater functionality in portable consumer electronic products, electromigration is becoming a current serious reliability issue. This is because of the increase of current density to be carried by the power solder joints (Tu, 2010).

The eutectic tin–lead (Sn-Pb) has a melting point of 183◦C. The ability to form a metallic bond with Cu substrate at such a low temperature is the key reason to used Sn-Pb solders worldwide for so long (Tu, 2010). Because of the miniaturization trend in the electronic devices, their requires smaller solder joint and fine pitch interconnections (Shen and Chan, 2009). On the other hand functional density enhancement and reliability issue are the key concerns in the electronic industries for the market demand. Therefore ball grid array (BGA) and flip chip (FC) packaging technologies are being used in the electronic industries for having higher input/output connections in a certain area (Arden, 2002). High localized temperature during service as a result of ultra-fine solder joints in BGA and FC packaging leads to coarsening the solder microstructure and deteriorate the reliability. It has become the main technological issue for electronic packaging and soldering. A typical FC and BGA package is shown in Figure 2.1.

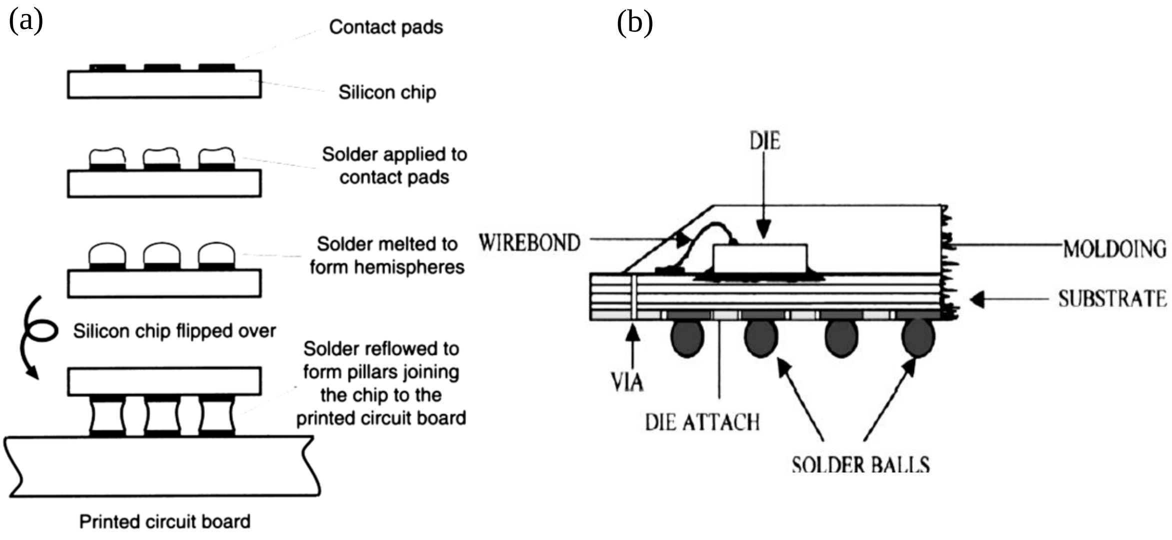

Figure 2.1:a) Schematic illustration of the flip-chip joining process (Humpston and Jacobson, 2004) b) Cross-section of a ball grid array (BGA) microelectronic component (Abtew and Selvaduray, 2000).

Reflow and wave soldering processes are being used in the electronic industries for the preparation of solder joints (Suganuma, 2001). In reflow soldering process solder is applied as paste by using a stencil mask and then heated to the reflow temperature. This soldering process is quite common in surface mount technology (SMT) process on printed circuit boards (PCBs) (Jianbiao et al., 2004).Wave soldering is also used for pin-in-hole (PIH) or pin-through-hole (PTH) types of assemblies where molten solder is used in the bottom side of PCB and then heated to the reflow temperature. Selection proper material for technological demand and reliability is very crucial in both reflow and wave soldering process. In the near future it is required to overcome more challenges for manufacturing of miniaturized, higher performance and multifunctional electronic device, especially in the metallurgical aspects.

2.2 Key parameters of soldering

The quality of soldered joints depends strongly on the combination of filler and component materials, including surface coatings that may be applied to the components, and also on the processing conditions that are used. The key parameters of soldering include surface energy and surface tension, wetting and contact angle, fluid flow, filler spreading characteristic, surface roughness of component, dissolution of parent materials, intermetallic growth, significance of joint cap and the strength of metal (Humpston and Jacobson, 2004).

2.2.1 Wetting and contact angle

According to the classical model of wetting, the liquid will spread over a solid surface until the three surface tensions (between the liquid droplet and the solid substrate, the liquid droplet and the atmosphere, and the substrate and the atmosphere) are in balance as shown in Fig. 2.2.

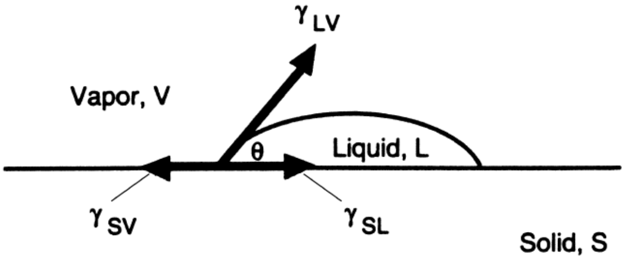

Figure 2.2 surface tension forces acting when a liquid droplet wets a solid surface, according to the classical model

According to the balance of forces:

$$\gamma_{sl} = \gamma_{sv} - \gamma_{lv} \cos\theta \tag{2.1}$$

Where γ_{sl} is the surface tension between the solid and liquid, γ_{lv} is the surface tension between the liquid and vapor, γ_{sv} is the surface tension between solid and vapor, and θ is the contact angle of the liquid droplet on the solid surface.

Equation 2.1 is called the wetting or Young's equation which shows that $\theta < 90°$ corresponds to the condition $\gamma_{sv} > \gamma_{sl}$.The driving force for the spreading of liquid over the solid surface and reduction in size of the un-wetted surface area is provided by the imbalance in surface tension.

The contact angle θ provides a measure of the quality of wetting. If $90° < \theta < 180°$, some wetting is said to occur, but a liquid droplet will not spread on the surface with which it is in contact. If $\theta < 90°$, a liquid droplet will wet the substrate and also spread over an area defined by the contact angle θ (de Gennes, 1985).

2.3 Health and Environmental Effects of Pb

Pb is one of the top 17 chemicals posing the greatest threat to human life and the environment on the basis of the United States Environmental Protection Agency (USEPA) (Wood and Nimmo, 1994). Pb in the electronic industries is considered as hazardous material for the environment. Wastes of electronic products are usually disposed to the landfills contaminates the soil, water, human body and food-chain in ecosystem (Glazer, 1994). Therefore "green" electronic products completely free of toxic materials such as Pb are being widely grabbed researcher's attention (Harrison et al., 2001).

Because of the mentioned state, a bill to ban Pb from all electronic materials was introduced in the US court in 1990, but it was opposed by the industries because of having no alternative solution to replace Pb. On the other hand, the European Union (EU) put their effort to recycle the lead products. According to the EU directives on Waste Electrical and Electronic Equipment (WEEE) imposed a rule that all products should be Pb-free from 2008 (COM, 2000). The RoHS directives (restriction of hazardous substance directives) rigidly restrict the use of Pb from all electronic components. But for many applications in electronic products, there is not found any other option or "drop-in" solution for the replacement of Pb from electronic components yet. All major manufacturers of electronic components planned to eliminate Pb from their products and seriously looking for an alternative option.

2.4 Lead Free Solder Candidates

Nearly all the eutectic Pb-free solders are Sn-based. A special class of them are the eutectic alloys consisting of Sn and other metals such as Au, Ag, Cu, Bi, In, Zn, Sb, and Ge have been considered. The eutectic points of the binary Pb-free solder systems are compared with that of eutectic Sn-Pb is shown in Table 1.1. It can be seen that there is a large temperature gap between the eutectic temperatures of Pb-free alloys with the Pb-Sn eutectic solders (exception Sn-Zn system:198.5◦C) (Tu, 2010).

A great deal of effort has been put into the development of Pb-free solder alloys. Pb-free solders should have certain criteria to use. Physical reliability, temperature requirements, compatibility with parts and processes, repairs and rework, low cost are the most important criteria. There are several Pb-free solders for different applications in the electronic industry , such as, Sn-Au, Sn-Bi, Sn-Zn, Sn-In, Sn-Ag, Sn-Cu, Sn-Ag-Cu etc. which have been examined. The main characteristics of these solder alloy are discussed below.

Table 2.1 Binary Pb-free eutectic solders (Tu, 2010).

system	Eutectic temp. (°C)	Eutectic composition
Sn-Cu	227	0.7
Sn-Ag	221	3.5
Sn-Au	217	10
Sn-Zn	198.5	9
Sn-Pb	183	38.1
Sn-Bi	139	57
Sn-In	120	51

Zinc (Zn) is cheap and easily available, but it quickly forms a stable oxide, resulting in unreasonable drossing during wave soldering, and also it shows very poor wetting behavior due to the stable oxide formation. Hence, a forming gas ambient is required. The eutectic Sn-Zn has a melting point which is closest to that of eutectic Sn-Pb among all the eutectic Pb-free solders and it has received much attention in Japan, especially.

Bismuth (Bi) has very good wetting properties. The eutectic Sn-Bi solder has been used in pin-through-hole technology. However, the availability of Bi could be limited by the restrictions on Pb, because the primary source of Bi is a by-product in Pb refining. By restricting the use of Pb, much less Bi will be available. Antimony (Sb) has been identified as a harmful element by the United Nations Environment Program. Germanium (Ge) is used only as a minor alloying element of multicomponent solders due to its reactivity. Indium (In) is too scarce and too expensive to be considered for broad applications, besides it forms oxides very easily.

A common characteristic of eutectic Sn-noble metal alloys is the high melting point and high concentration of Sn compared to that of eutectic Sn-Pb. For this reason the reflow temperature will be higher, by about 40°C. It may increase the dissolution rate and solubility of Cu and Ni in the molten solder as well as the rate of intermetallic compound (IMC) formation with Cu and Ni under-bump metallization. If the surface and interfacial energies are considered, the surface energies of these Pb-free solders are higher than that of Sn-Pb, so they form a larger wetting angle on Cu, about 35 to 40°.

Concerning the microstructure of these eutectic solders, they are a mixture of Sn and IMC because of the high concentration of Sn, unlike that of eutectic Sn-Pb which has no IMC. Since metallic Sn has the body-centered tetragonal lattice structure and tends to deform by twinning, its mechanical properties are anisotropic. The electrical conductivity of metallic Sn is also anisotropic. The mechanical and electrical properties of these eutectic solders will be anisotropic, thus the dispersion of the IMC may lead to the formation of inhomogeneous microstructures, especially in the case of Ag_3Sn. The image of Ag_3Sn appears to be long needlelike crystals in the eutectic Sn-Ag on the cross-sectional image of a solder joint. But after the matrix of the solder is removed by deep etching, they turn out to be plate-like.

2.4.1 Sn-Au

Among all the Pb-free solders, Au-based solder has been found as one of the most environmental friendly solder and it is being used in the semiconductor industry for the assembly process (Liu et al., 2008). Au has been ranked among the least toxic elements by both EPA-US (Environmental Protective Agency-United States) and OSHA (Occupational and Safety Health Administration). The eutectic 80Au-20Sn solder has excellent high-temperature performance, superior resistance to corrosion, high electrical and thermal conductivity and offers fluxless soldering. But, the hardness decreases, creep penetration and creep strain rate of Au-based solder increase with temperature (Chidambaram et al., 2010). Beside this, Au-based solder possess acceptable properties such as suitable melting temperature, good thermal and electrical conductivities, good fluidity and wettability. However, the alloy system has some problems such as low ductility and high cost, which prevent its wide application (Takaku et al., 2008).

2.4.2 Sn-Bi

The eutectic Sn-58Bi solder offer a lower melting point than Sn-Pb alloys of 139°C. The cost of bismuth is almost similar to that of tin (Abtew and Selvaduray, 2000). There is a problem to supply it because it is a by-product of Pb mining. If a bismuth alloy picks up any Pb, the melting temperature will drop again with the formation of another secondary eutectic formed at 96°C (Suraski and Seelig, 2001). Beside this, bismuth soldering alloys tends to create embrittlement (Wild, 1971). Bismuth alloys also are prone to failure in peel strength tests due to poor fatigue resistance. Bismuth is also a poor conductor, both thermally and electrically (Felton et al., 1993).

2.4.3 Sn-Zn

Zinc is a readily available metal and cheap. The eutectic Sn-9Zn alloy has a low melting point of 198ºC which is the closest to eutectic Pb-Sn solder among all other lead-free alternatives (Abtew and Selvaduray, 2000). For this reason, in the recent years the Sn-9Zn alloy received much attention to the electronic industries. But zinc shows a very poor wetting behavior with the substrate including poor corrosion resistance in humid or high temperature environment and forms a stable oxide which keeps its use limited in the electronic packaging industries (Liu and Tu, 1998, Liu et al., 2008).

2.4.4 Sn-In

The eutectic Sn-52In alloy has a relatively low temperature of 120ºC (Korhonen and Kivilahti, 1998), which makes this solder suitable for low temperature applications. This alloy is a good choice for temperature sensitive equipments which are not exposed to any harsh or high-stress environments. But indium is a rare metal and too expensive to consider it for board applications (Sharif and Chan, 2005). Furthermore, In alloys suffers poor corrosion resistance, forms oxide very rapidly during melting and show strong segregation behavior in the liquid (Korhonen and Kivilahti, 1998).

2.4.5 Sn-Ag

The Sn-4Ag is a rather good alloy and has a long history in the hybrid circuit industries for electronic packaging applications. But the melting point of this alloy is 221ºC which is considered higher for many surface mount technology (SMT) applications.

2.4.6 Sn-Cu

The eutectic Sn-0.7Cu is another reliable solder alloy for reflow and wave soldering applications. The melting temperature of this solder is 227ºC which is undesirable in many reflow applications. Moreover, the microstructure of this alloy is prone to whisker growth because of high Sn concentration (Boettinger et al., 2005). The cost of this solder is much lower comparing other solders since it does not contain any expensive elements such as, Ag, Bi or In.

2.4.7 Sn-Ag-Cu

This family of Pb-free Sn-Ag-Cu alloys has shown high promise in the electronic industries due to having good wetting characteristics with substrate, good fatigue resistance, good joint strength etc. Owing to these advantages, in 2000 the National Electronic Manufacturing Initiative (NEMI) recommended to replace eutectic Sn-Pb solder by near eutectic Sn-Ag-Cu alloys.

Ternary and higher order solders are most likely based on the binary eutectic Sn-Ag, Sn-Cu, Sn-Zn, or Sn-Bi alloys. The most promising one is eutectic Sn-Ag-Cu. The eutectic Sn-Ag-Cu alloy forms good quality joints with copper. Its thermo-mechanical property is better than those of the conventional Sn-Pb solder. Its eutectic temperature has been determined to be about 217°C, but its eutectic composition has been a subject of controversy. Based on metallographic examination, differential scanning calorimetry measurements, and differential thermal analysis results, the eutectic composition was estimated at 3.5 ± 0.3 Ag, 0.9 ± 0.2Cu (wt%).

2.5 Thermodynamics of Sn-Ag-Cu Solder Alloy Selection

The phase transformation of Sn-Ag-Cu system is evaluated based on the following binary systems: Sn-Ag, Sn-Cu and Ag-Cu (Moon et al., 2000). The calculated binary phase diagrams for the binary system Sn-Ag, Sn-Cu and Ag-Cu are shown in Figure2.4.

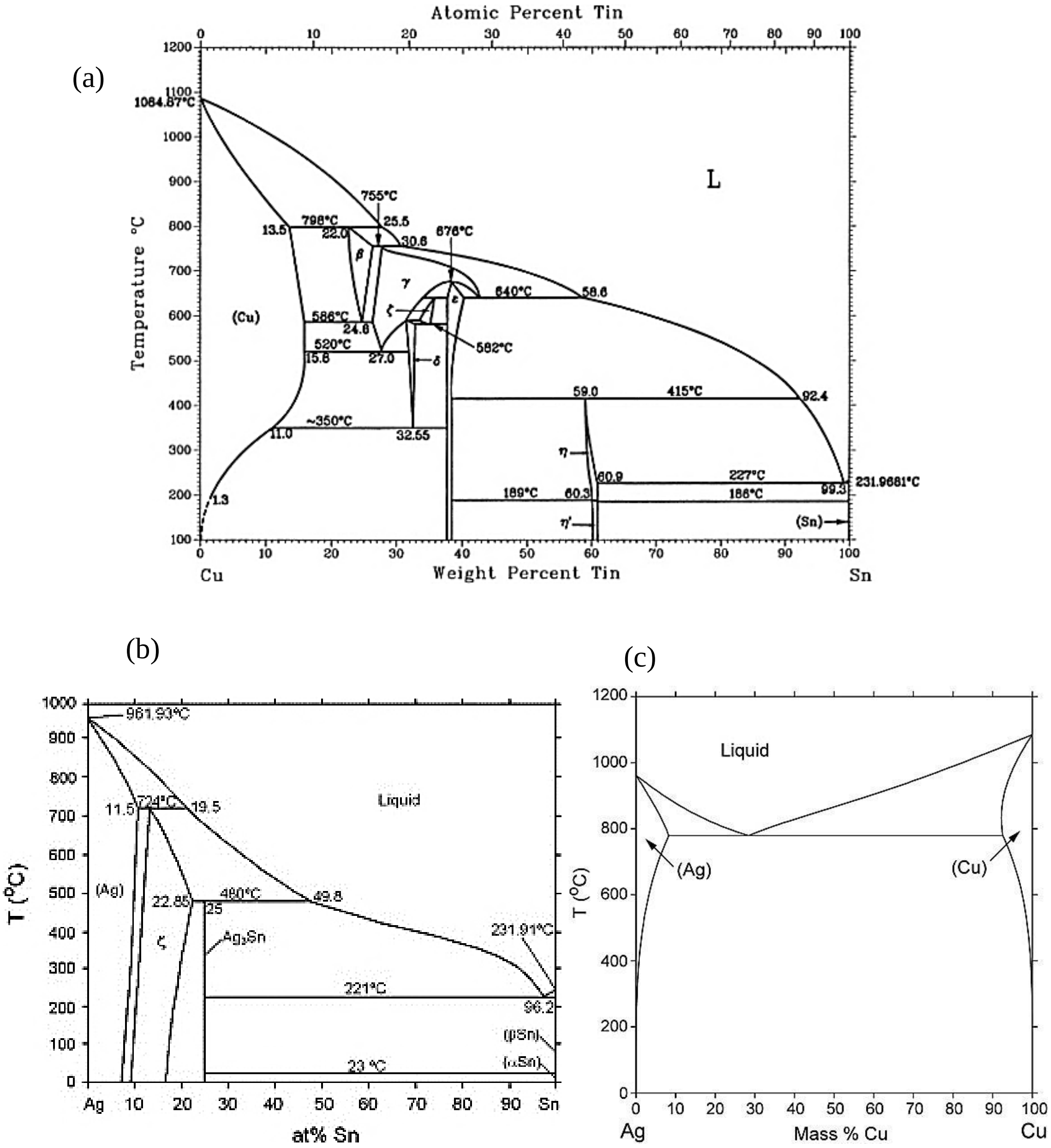

Figure 2.3 Phase diagram of the (a) Sn-Cu (Franke and Neuschütz, 2005), (b) Sn-Ag (Karakaya and Thompson, 1987) and (c) Ag-Cu system (Xie and Zhang, 1998).

The eutectic temperature of the Sn-Cu system is 227ºC. The eutectic composition is varied from 0.7 to 0.9 wt% Cu (Moon et al., 2000). The eutectic constituents obtained from the Sn-Cu phase diagram (Figure 2.3a) are β-Sn and Cu_6Sn_5 intermetallics. On the other hand, the eutectic composition of the Sn-Ag system is unanimously taken at 3.5 wt % of Ag and calculated eutectic temperature is 220.1ºC (Oh et al., 1996).

From the Sn-Ag phase diagram (Figure 2.3b), the eutectic constituents are β-Sn and Ag_3Sn intermetallics. Not all binary or ternary elements form the intermetallic compound in a binary or ternary alloy system. For example, in the Ag-Cu binary system there is no intermetallic compounds as it is seen in the Figure 2.3c.

These binary phase diagrams are used to understand the melting behavior of ternary Sn-Ag-Cu alloy. The alloy design criterion for the Sn-Ag-Cu alloy is as follows (Bath, 2010):

01. The liquidus melting temperature of the alloy should be close to the eutectic Sn- Pb alloy (183ºC) to avoid changing the manufacturing process, materials and infrastructure.
02. The gap between the solidus and liquidus temperature should be as low as possible to avoid tombstoning phenomenon and fillet lifting.
03. The solidus temperature of the solder should be significantly higher than the operating temperature of the solder.

The National Center for Manufacturing Sciences (NCMS), Michigan, USA suggested that the solder liquidus temperature should be less than 225ºC with a maximum 30ºC difference between solidus and liquidus temperature (Bath, 2010). Obviously the ternary eutectic or near eutectic Sn-Ag-Cu alloys meet the first two criterions since the melting temperature of the ternary eutectic Sn-Ag-Cu alloy is 217ºC (Moon et al., 2000). Depending on particular applications the operating temperature of electronic equipments may be as high as 150ºC (Suganuma, 2001). So the ternary eutectic or near eutectic Sn-Ag-Cu alloys are one of the best candidates for Pb-free solder alternatives. The calculated eutectic composition of the Sn-Ag-Cu system is 3.66 wt% Ag, 0.91 wt% Cu as it is seen in Figure 2.4. But the experimentally determined value of the Sn-Ag-Cu system is 3.5 wt% Ag, 0.9 wt% Cu which differs a little from the calculated value.

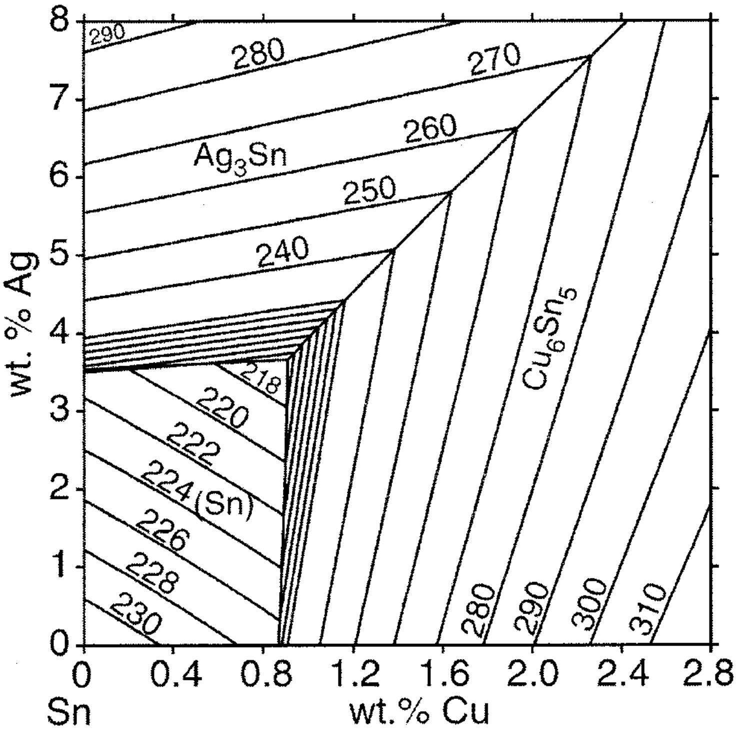

Figure 2.4 Calculated liquidus surface of the Sn rich region of Sn-Ag-Cu alloy system (Moon et al., 2000).

2.6 Phase Diagram of Mo with Sn, Ag and Cu

The phase diagrams of Mo with Sn, Ag and Cu are shown in the Figure 2.5(a-c) respectively. It is seen in the Mo-Sn phase diagram (Figure 2.5a) that Mo has no solubility in Sn at low temperatures (<300°C). The calculated results on solubility of Mo in Sn also show that there is a very negligible solubility of Mo in Sn (Brewer and Lamoreaux, 1980) . Three intermetallics e.g.$Mo_3Sn, Mo_2Sn_3/Mo_3Sn_2$and $MoSn_2$ can form in the Mo-Sn system below 300°C(Brewer and Lamoreaux, 1980). On the other hand, the Mo-Ag phase diagram (Figure 2.5b)(Baren, 1990) and Mo-Cu phase diagram (Figure 2.5c)(Subramanian and Laughlin, 1990) show that Mo has no solubility in Ag and Cu respectively. Besides, it is also revealed that Mo does not form any compound with Ag and Cu (Subramanian and Laughlin, 1990).

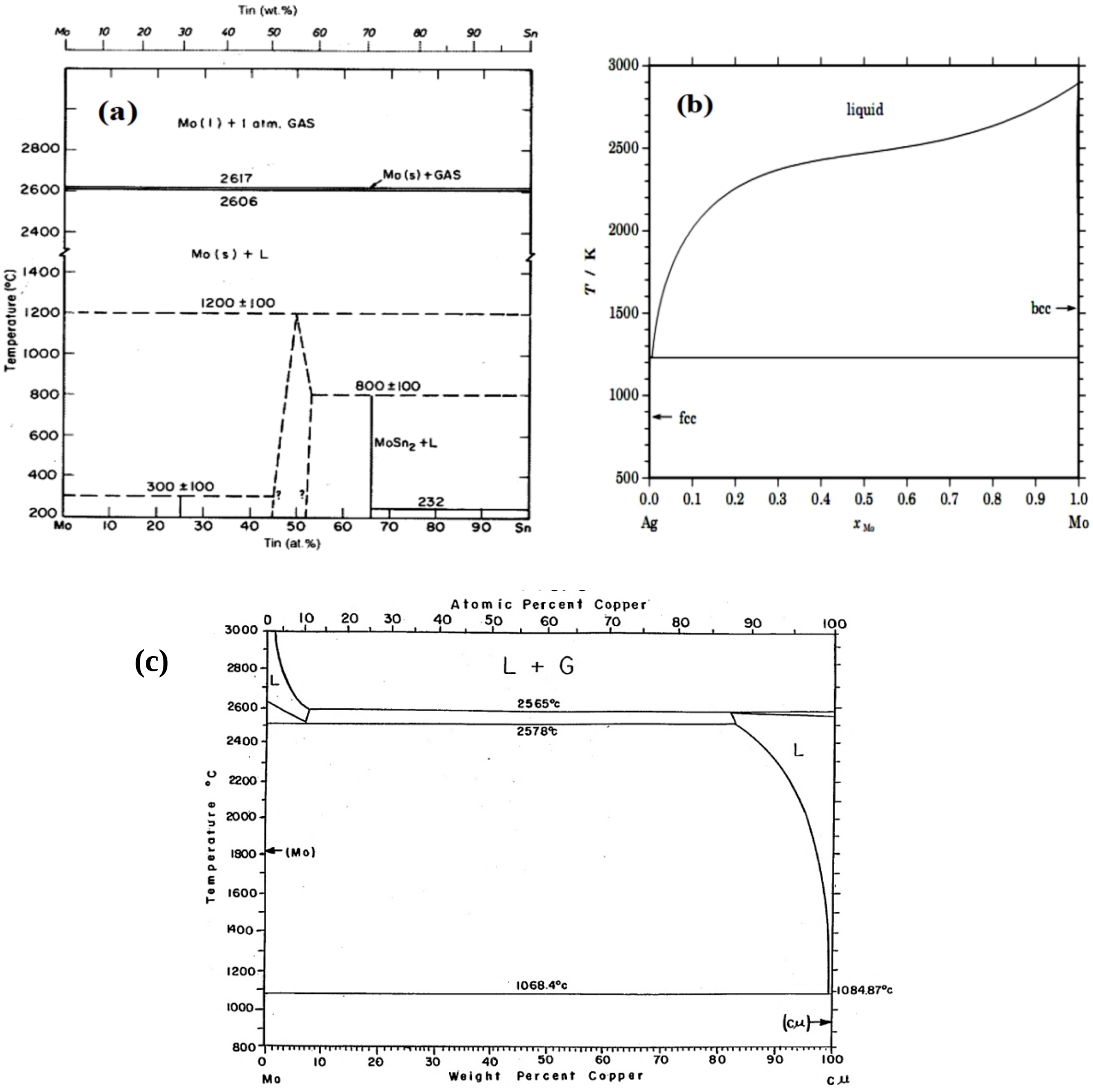

Figure 2.5Phase diagram of the (a) Mo-Sn (Brewer and Lamoreaux, 1980) b) Mo-Ag (Baren, 1990) and (c) Mo-Cu (Baren, 1990).

2.7 Interfacial Reactions of Sn-Ag-Cu Solder with Substrate

During the soldering process, reactions happen between the solder and substrate and intermetallic compounds (IMCs) form between them. For a good metallurgical bond it is essential to have a uniform IMC layer between the solder and substrate. However, the thickness of IMC strongly affects the reliability and mechanical properties of the solder joint. A thick IMC hamper the interface integrity because of its brittle nature and creates mismatch in physical properties such as elastic modulus, thermal expansion etc. For this reason, the interfacial reaction should be controlled to ensure the reliable properties of the solder. The interfacial reaction between the solder and substrate can be categorized into two groups, namely:

01. Reactions during reflow process,

02. Reactions during high temperature aging.

The former process is encountered during the reflow and wave soldering processes and the latter happens during service or high temperature aging test.

2.7.1 Microstructure of Interfacial IMCs during reflow

Formation of intermetallic compounds is inevitable during soldering reaction between the molten solder and substrate. An adequate and uniform intermetallic layer is essential for a good metallurgical bond between the solder and substrate. But the inherent brittle nature of interfacial IMCs promotes a brittle failure to the interface (Lee et al., 1997, Pang et al., 2004b). For this reason, the thickness of the interfacial IMC should be optimized. During service or high temperature aging the thickness of interfacial IMC increases due to diffusion of Sn from the bulk solder to the substrate (Sivasubramaniam et al., 2008).

Solder alloys melt and then react with the substrates to form IMCs, such as Cu_6Sn_5, Cu_3Sn, Ni_3Sn_4 and $(Cu,Ni)_6Sn_5$ at the solder/substrate interface during soldering (Laurila et al., 2005). Forming a thin IMC layer by the interfacial reactions is desirable to achieve a good metallurgical bond; however, excessive IMC growth may have a harmful effect (Müller, 2004). Therefore aging degradation of the solder joint in electronic packaging is a critical concern in microelectronic industry. Furthermore, the addition of certain trace amount alloying elements has strong effects on IMC growth behaviors (Laurila et al., 2009). For example, the Ni-based substrates were more effective than Cu in reducing the growth rate of IMCs, as Ni_3Sn_4 was formed during the interfacial reactions with Ni-based substrates (Rizvi et al., 2007).

Both Cu and Ni thin films are used widely as on-chip under-bump metallization (UBM), but they can be reacted and dissolved away by molten solder during reflow, resulting in spalling of IMC. Hence, a solder of eutectic composition is undesirable when it is used with thin-film UBM. It must be supersaturated with excess Cu and/or Ni, about 1%, in order to reduce the dissolution. Therefore, the recommended composition for Sn-Ag-Cu solder is about Sn-3Ag-3Cu. While it is off the eutectic composition and will not have a single melting point, the effect of the composition on melting temperature is very small and will not be an issue in manufacturing.

2.7.1.1 Sn–Ag–Cu/Cu

Cu is the most common conductor metal, which is utilized in contact with solders owing to its good solderability characteristic and excellent thermal conductivity performance (Rizvi, Chan et al. 2006).

The whole interfacial layer of the IMCs will trend to become planar with increasing reflow time (Moon et al., 2000). The IMC layer are composed of two layers, the light gray regions are Cu_6Sn_5 and thin dark gray layer beneath is Cu_3Sn, the thickness of which is very thin, as shown in figure 2.7 (Peng et al., 2007).

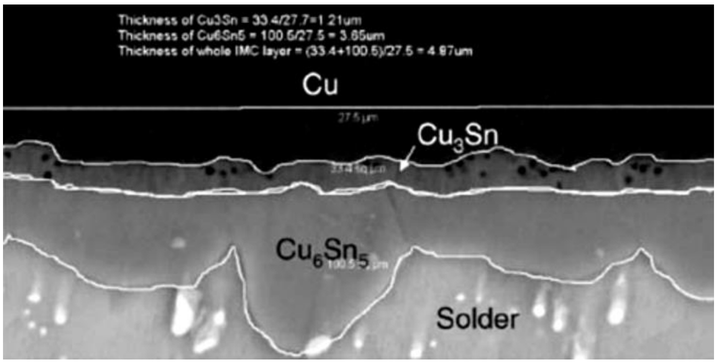

Figure 2.6 IMC layers formed between the solder and Cu substrate after soldering (Zhang et al., 2009).

Figure 2.7 (a) and (b) shows the IMC layers morphology formed between the solder and Cu substrate after soldering, which presents the interface morphology of the IMCs layer under reflow durations (Zhang et al. 2009). The atomic-percentages of Cu and Sn in Cu_6Sn_5 phase are 55 and 45, respectively (Kim et al. 2002).

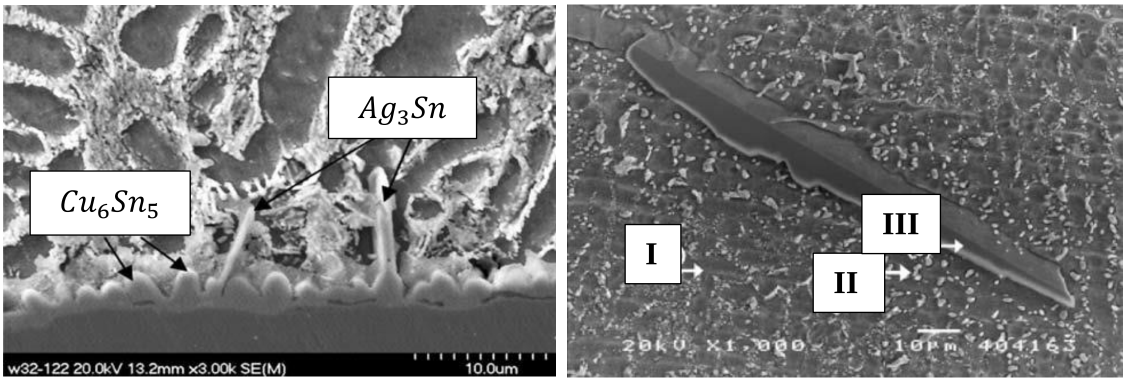

Figure 2.7(a) The microstructure of IMC layer at the interface between solder and Cu (Zhang et al., 2009). (b) SEM image of typical microstructure of Sn–Ag–Cu solder I)Sn-rich, II) Cu_6Sn_5, and III) Ag_3Sn (Pang et al., 2004a).

Formation of Cu_6Sn_5 IMC during the reaction between molten Sn-based solder and Cu substrate has been reported by a number of studies (Gong et al., 2009, Laurila et al., 2005). Some of the study also reported the formation of a very thin Cu_3Sn layer (a few tens of nanometer) between the Cu_6Sn_5 IMC and Cu substrate (Gong et al., 2009, Shang et al., 2009). But after reflow most of the time this thin Cu_3Sn layer is not visible under SEM in the cross-sectional view. In general, for most of the Sn-based solder this newly form Cu_3Sn IMC layer grows at the side of Cu substrate during reflowing (Tu, 2010).

Moreover, Ag_3Sn IMC was found dispersed uniformly in the solder after reflow. The planar Ag_3Sn which formed near the interface have changed remarkably and merged together to large platelets with increasing thermal cycles or aging (Pang et al., 2004a). Large Ag_3Sn needles can cause reliability concern when they form in a high stress concentration area, such as the corner between solder and copper substrate. Fatigue cracks can initiate and propagate along the interface between the Ag_3Sn and solder matrix, as leading to mechanical failure (Schoeller et al., 2009).

2.7.1.2 Sn–Ag–Cu/Ni

In electronic products, Ni is one of the most common metals to be in direct contact with the solders. Nickel is used as a solderable diffusion barrier in several types of surface finishes for components and printed circuit boards, since the reaction rate of Ni with molten solder is typically smaller than that of Cu. Therefore, the interactions between Ni and the Sn-Ag-Cu solders must be understood (Ho et al., 2002).

Sn–Ag–Cu solder reflowed on pure Ni substrates showed distinctly different from those observed for Sn–Ag–Cu/Cu solder joints, as revealed in Fig.2.8. Instead of Ni_3Sn_4, it was determined by means of WDS (Wavelength-Dispersive X-Ray Spectroscopy) analysis that a different phase was growing at the interface, with a composition of $Cu_xNi_ySn_{45}$, where the Cu concentration X varied between 44 and 53 atomic percent, and the Ni concentration y between 1 and 10 atomic percent. These compositions are consistent with the stoichiometry of the compound $(Cu,Ni)_6Sn_5$ (Zribi et al., 2001).

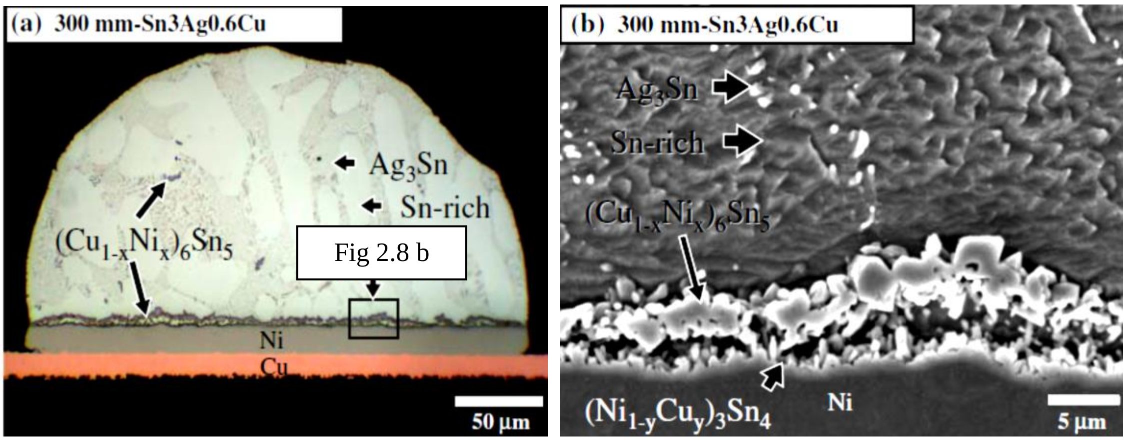

Figure 2.8(a) Interface between Sn-3.0Ag-0.6Cu solder ball and Ni/Cu substrate (b) Zoom-in view of (a) (Ho et al., 2007).

The reaction between Ni and two solders (Sn3.9Ag0.2Cu and Sn3.9Ag0.6Cu) has been reported to be very sensitive to the Cu concentration in the solder (C. Ho, et al., 2002). When Sn3.9Ag0.2Cu reacted with Ni, a continuous $(Ni_{1-x}Cu_x)_3Sn_4$ intermetallic layer formed at the interface. In contrast, when Sn3.9Ag0.6Cu reacted with Ni, a continuous

$(Cu_{1-y}Ni_y)_6Sn_5$ intermetallic layer formed. These two compounds, $(Ni_{1-x}Cu_x)_3Sn_4$ and $(Cu_{1-y}Ni_y)_6Sn_5$, are based on the Ni_3Sn_4 and Cu_6Sn_5 crystal structures, respectively.

In Figure 2.9 (a) and (b) shows the phase diagram of Cu-Sn and Ni-Sn respectively. Only a section of the ternary phase diagram of the Cu– Ni–Sn system is available at 235℃ based on experimental data and thermodynamic modeling as shown in figure 2.9(c) (Korhonen et al., 2000). The $(Cu,Ni)_6Sn_5$ band $(Ni,Cu)_3Sn_4$ compounds are presented in this diagram as narrow composition range compounds which extend the domain of the respective binaries Cu_6Sn_5 and Ni_3Sn_4 to a ternary domain. The Cu–Ni–Sn phase diagram also displays a large two-phase region between $(Cu,Ni)_6Sn_5$ and the Cu–Ni solid solution and a three-phase region between $(Cu,Ni)_6Sn_5$ $(Ni,Cu)_3Sn_4$, and the Sn–Cu–Ni solid solution. These observations support the idea of a substitutional mechanism where atoms such as (Cu and Ni) and (Ni and Au) substitute for each other in their binary compounds with Sn (Lee et al., 2003).

Both the Cu concentration and the solder volume had a strong effect on the type of the reaction products (Ho et al., 2006). In detail $(Cu,Ni)_6Sn_5$ massively spalled from the interface under certain conditions, including smaller joints and those with lower Cu concentration. The massive spalling of $(Cu,Ni)_6Sn_5$ was attributed to the decrease of the available Cu in the solders (Lin and Shih, 2008). The results of this study suggest that Cu-rich Sn–Ag–Cu solders can be used to prevent this massive spalling.

The evolution of intermetallics are examined at and near SnAgCu/Cu and SnAgCu/Ni interfaces, and explains that the presence of the Cu in the solder dramatically altered the phase selectivity at the solder/Ni interface and affected the growth kinetics of intermetallics. As long as sufficient Cu was available, it would combine with Ni and Sn to form $(Cu,Ni)_6Sn_5$, which grew instead of the Ni_3Sn_4. This growing phase would, however, eventually consume essentially all of the available Cu in the solder (Zribi et al., 2001). Because the mechanical properties of Sn–Ag–Cu alloys depend upon the Cu content, this consumption can be expected to alter the mechanical properties of these Pb-free solder joints.

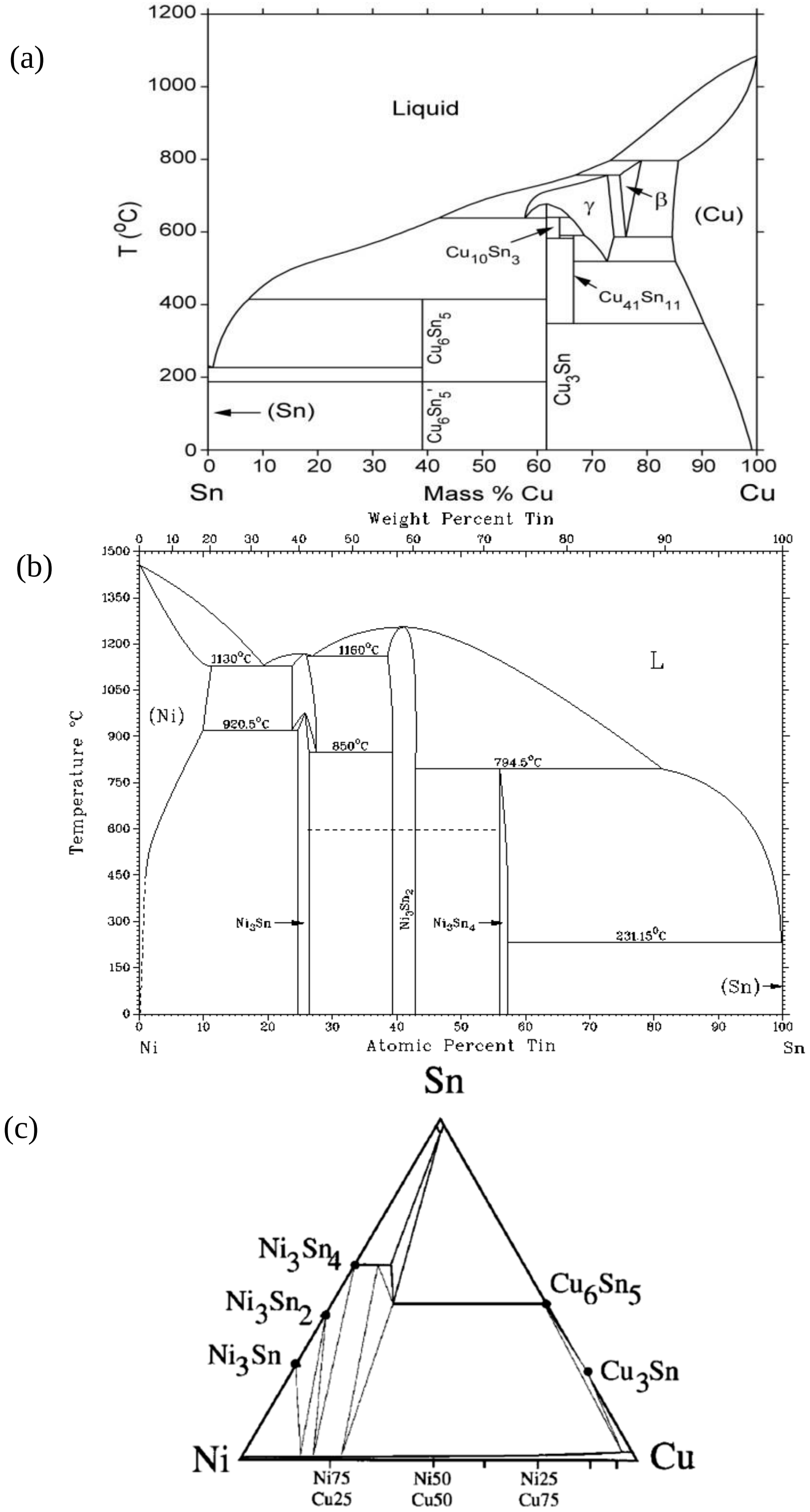

Figure 2.9 (a) Phase diagram for system Cu-Sn (Franke and Neuschütz, 2005) (b) Phase diagram of Ni-Sn (Okamoto, 2006) (c) Partial phase diagram of the Cu-Ni-Sn system at 235°C. It can be seen that the $(Cu,Ni)_6Sn_5$ compound extends to a wide range of ternary compositions (Korhonen et al., 2000).

2.8 Nucleation and Growth of Interfacial IMCs

In the eutectic Sn-Ag-Cu system, the undercooling for the nucleation of the solid Ag_3Sn phase is small, 7.2 °C with differential scanning calorimetry (DSC) in the Sn-3.8Ag-0.7Cu alloy. But the formation of the Ag_3Sn does not facilitate the nucleation of the β-Sn phase. The β-Sn does not wet on the previously formed Ag_3Sn, therefore; it will not nucleate heterogeneously on the Ag_3Sn. The undercooling for the β-Sn phase is 29 °C in the same alloy. It was observed that the large undercooling of the β-Sn phase in the presence of large Ag_3Sn intermetallic particles and the same conclusion was reached, that the intermetallics particles are ineffective as heterogeneous nucleation substrates for Sn (Moon et al., 2000).

The eutectic Sn-3.5Ag, Sn-0.7Cu, and Sn-3.5Ag-0.9Cu alloys are anomalous. The difference in the melting point between Sn and Ag (or Cu) is large; the difference in the volume fraction of the constituent phases, β-Sn and Ag_3Sn (or Cu_6Sn_5), is also large. More importantly, the Ag_3Sn and Cu_6Sn_5 are faceting phases, while β-Sn is a non-faceting phase. During solidification, the faceting phase, Ag_3Sn or Cu_6Sn_5, grows by layer deposition involving the lateral propagation of a step across the liquid/solid interface. On the other hand, the non-faceting phase, β-Sn, advances into the liquid phase by tree-like, non-faceted dendrites. Because of the different growth mechanisms, the growth rates of the β-Sn and Ag_3Sn (or Cu_6Sn_5) are quite different. Therefore, the growths of the β-Sn, and Ag_3Sn (or Cu_6Sn_5) are independent or only loosely coupled (Shangguan, 2005).

2.8.1 Formation Mechanisms of Interfacial IMCs

The formation of IMC layer is mainly due to the diffusion of atoms from the substrate into the solder matrix (Yoon et al., 2008). IMCs form instantly at the interface and serve as the bonding materials between the solder and the substrate as well (Li et al., 2005).

Transferring through the solder/flux interface was considered as the major mechanism, which is demonstrated by means of EDX analysis. During wetting, Sn in the solder and Cu in the substrate begin to move into the flux. The rate of this transport is low because the ball and the substrate are in solid state. So the transportation zones (TZs) for Sn and Cu are still very thin and close to the solder and the Cu substrate, as illustrated in Fig. 2.10a. No obvious interfacial reactions were observed. As the temperature increasing and the solder ball molten, the transfer rate of Cu is still low, and its TZ is still thin and close to the substrate. In contrast, the transfer rate of Sn from the molten solder is considerably higher. This results in a much thicker layer of Sn–TZ around the molten solder ball, as illustrated in Fig. 2.10b. When the Sn–TZ meets with the Cu–TZ, the formation of reactants was initiated. As shown in Fig. 2.10b, the overlap area determines the morphology of fine Cu_3Sn-particles layer (Gong et al., 2009).

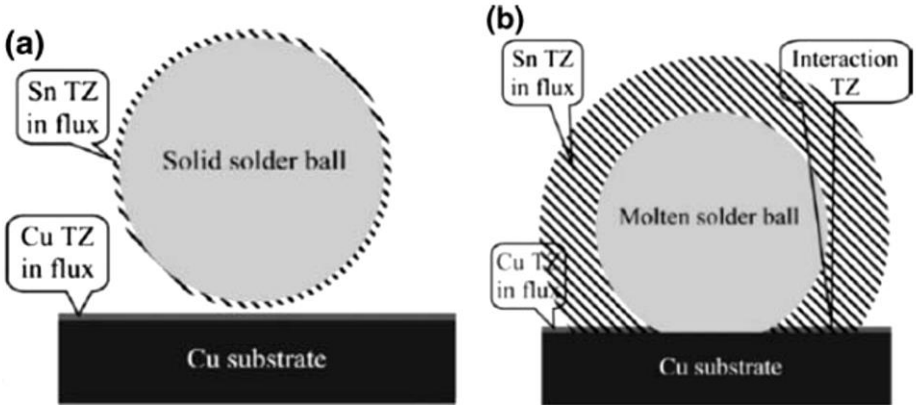

Figure 2.10 Formation mechanism of the fine Sn–Cu particles layer near the three-phase contact line: a low temperature and b high temperature with the molten solder ball (TZs transportation zones).

In summary, the surface of Cu is modified by a layer of Cu–Sn IMCs in front of the three-phase contact boundaries during the wetting process. The liquid solder then spreads and covers over the existing Cu_3Sn layer, forming the $Cu_6Sn_5/Cu_3Sn/Cu$ sandwich structure interface. To form the Cu_3Sn transition zone, both Cu and Sn are required. Cu can be mainly supplied by the Cu substrate. Sn may transport through the flux to the transition zone.

2.9 Effects of Alloying Elements on the Interfacial IMCs

A good deal of work has been done on the interfacial IMCs with the addition of alloying elements. Based on a summary of the previous research, the addition of alloying elements to the solder can affect the interfacial IMCs in the following three ways (Zeng et al., 2010):

1. Alloying elements can increase or decrease the thickness of interfacial IMCs.
2. The physical and chemical properties of the interfacial IMCs can be altered due to the addition of alloying elements.
3. Additional reaction layer can form at the interface between the solder and substrate.

Alloying elements can be categorized in two groups on the basis of solubility (Laurila et al., 2010):

1. Elements that show marked solubility on the Sn-Cu intermetallics, such as Ni, Co, Au, Sb, In, etc.
2. Elements that do not show marked solubility on the Sn-Cu intermetallics, such as Al, Bi, P, Ti, S, rare earth elements.

Between alloying elements, Ni and Co has a prominent solubility on the interfacial IMCs. It is found that the addition of Ni and Co as an alloying element to the solder increases the total IMC thickness but the Cu_3Sn IMC thickness is decreased during reflow and aging compared to the pure solder (Wang et al., 2009). It is observed that the addition of Au (less than 0.25 wt %) to the near eutectic SAC solder results scallop type $(Cu,Au)_6Sn_5$ IMC after reflow. However, if the Au content is more than 0.25 wt% the morphology of the interfacial IMC is changed with the formation of two phase layer $[((Cu,Au)_6Sn_5)+Sn]$ (Park et al., 2003). The addition of Au reduces the Cu_3Sn IMC, but the effect of Au is weaker compared Ni and Co because of having lower solubility in Cu_3Sn IMC (Zakel et al., 1991). On the contrary, though Sb has a strong effect on solid solution strengthening of Sn, it has virtually no effect on the interfacial IMC (Laurila et al., 2010).

Addition of elements that do not show marked solubility on the interfacial Cu-Sn IMC like Al is found to increase the mechanical properties such as microhardness, strength etc. to the SAC solder (Liu et al., 2008).

2.10 Effects of Nanoparticles on Interfacial IMC

In recent research, Nano-composite solders are being investigated specially for cases where better creep and fatigue resistance are required (Shen and Chan, 2009). Several methods such as ball milling, paste mixing, mixing with molten solder alloy, in-situ method have been developed for mixing nanoparticles with the solder (Hwang et al., 2003, Lin et al., 2002, Shen and Chan, 2009). Refinement of solder microstructure resulting from nanoparticle addition has been reported in a number of studies (Kumar et al., 2008, Shen et al., 2006). The effect of Co, Ni, Pt, Al, P, Cu, Zn, Ge, Ag, In, Sb and Au nanoparticles Studied on the interfacial IMC between Sn–3.0Ag solder and organic solderability preservative (OSP) Cu pads during reflow and aging process. It was also found that nanoparticles of Co, Ni and Pt are effective in influencing the growth of interfacial IMC layer between Sn-based Pb-free solder and Cu substrate after reflow(Amagai, 2008). Recent results show that Co and Ni nanoparticles impart their effect on the interfacial IMC through alloying effect (Amagai, 2008, Haseeb and Leng, 2011). With the addition of Co and Ni nanoparticles to the SAC solder the total thickness of interfacial IMC increases but the thickness of Cu_3Sn IMC decreases (Haseeb and Leng, 2011). Extent of alloying effect of nanoparticles is related to the solubility of that particular element into the solder (Laurila et al., 2010).

Reported results of inert nanoparticles addition to Sn-based solder such as Al_2O_3,SiC, TiO_2, carbon nanotube shows refinement bulk microstructure and improvement of the mechanical properties such as micro hardness (Shen and Chan, 2009). Inert nanoparticles are considered as a surface active material since they gather at the grain boundaries of the solder matrix and do not react with the solder. Surface absorption theory can be applied to explain the controlling mechanism of the suppression of interfacial IMC due to the addition of inert nanoparticles. According to the theory, the surface free energy of a whole crystal is:

$$\sum_k {\gamma_{(c)}}^k A_k = \sum_k {\gamma_{(0)}}^k A_k - \mathrm{RT} \sum_k A_k \int_0^c \frac{\Gamma^k}{c} \mathrm{dc} \qquad (2.2)$$

Where, Γ^k is the adsorption of surface-active material at crystal planes k, c is the concentration of the surface-active material, R is the ideal gas constant, T is the absolute temperature, ${\gamma_{(c)}}^k$ is the surface tension of crystal planes k with adsorption of the active material, ${\gamma_{(0)}}^k$ is the surface tension of the initial crystal planes k without adsorption, and A_k is the area of the crystal planes k.

The net value of the right hand side becomes lower with increasing the value Γ^{k}. This implies that the surface free energy of the whole crystal plane would decrease with the maximum amount of adsorption, Γ^k. Thus, an increase in the amount of elements adsorbed decreases its surface energy and, therefore, decreases the growth velocity of this crystal plane (Shen and Chan, 2009). Generally, crystal planes having higher surface energy grows rapidly. But the surface energy is deceased when surface active materials are absorbed at the crystal plane. As the amount of absorption of surface active material is increased, the growth velocity of the crystal plane is decreased.

The explanation in surface absorption theory is qualitative, thus this theory is not universally accepted to explain the effect of inert nanoparticles on the interfacial IMC. There are several factors that affect the growth process of interfacial IMCs, such as substrate dissolution, grain boundary diffusion, grain coarsening, grain boundary grooving etc., into the molten solder (Schaefer et al., 1998). So this is particularly important to investigate the distribution, locations, reactions of the nanoparticles into the solder during reflow (Shen and Chan, 2009).

2.11 Electrodeposition of Nickel

Nickel electroplating is a commercially important and versatile surface-finishing process. Its commercial importance may be judged from the amount of nickel in the form of metal and salts consumed annually for electroplating, now roughly 100,000 metric tons worldwide, as well as its versatility from its many current applications (DiBari, 1996).

Nickel electroplating is similar to other electrodeposition processes that employ soluble metal anodes; that is, direct current is made to flow between two electrodes immersed in a conductive, aqueous solution of nickel salts. The flow of direct current causes one of the electrodes (the anode) to dissolve and the other electrode (the cathode) to become covered with nickel. The nickel in solution is present in the form of divalent, positively charged ions (Ni^{+2}). When current flows, the positive ions react with two electrons ($2e^-$) and are converted to metallic nickel (Ni^0) at the cathode surface. The reverse occurs at the anode where metallic nickel is dissolved to form divalent, positively charged ions which enter the solution. The nickel ions discharged at the cathode are thus replenished by those formed at the anode (Schlesinger, 2010).

The amount of nickel deposited at the cathode and the amount dissolved at the anode are directly proportional to the product of the current and time and may be calculated from the expression (Faraday's Laws):

$$\mathrm{m}=1.095 \times aIt \tag{2.3}$$

Where m is the amount of nickel deposited at the cathode (or dissolved at the anode) in grams, I is the current that flows through the plating tank in amperes, t is the time that the current flows in hours, and a is the current efficiency ratio. The cathode efficiency of different nickel plating solutions may vary from 90 to 97% and, accordingly, a will vary from 0.90 to 0.97. Because the anode and cathode efficiencies are not exactly equal, the nickel ion concentration and the pH of the solution will slowly increase as plating proceeds.

2.11.1 Average Coating Thickness

An expression for calculating nickel thickness, s in micrometers, can be derived by dividing Eq. (2.4) by the product of the density of nickel, d (8.907 gcm^{-3}), and the surface area to be electroplated, A, and multiplying by 100 to obtain the thickness in micrometers:

$$s = \frac{m \times 100}{dA} = \frac{109.5 \times aIt}{8.097A} = \frac{12.294 \times aIt}{A} \qquad (2.4)$$

The ratio I/A is the current density and thus the above expression shows that the coating thickness depends on the current density and time, whereas the amount or mass of nickel deposited, Eq. (2.4), depends on the current and time. Equation (2.4) is the basis for the electrodeposition data compiled in Table 2.2, which gives the time in minutes required to deposit a nickel coating of specified thickness at different values of current density. The expression above and Table 2.2 provide a means of estimating the average coating thickness.

Table 2.2 Nickel Electrodeposition Data (Mordechay Schlesinger, 2010)

Deposit thickness (µm)	Weight per Unit Area(g	Ampere Hours per Unit (Ah dm^{-2})	Times (min) to obtain Deposit at Various Current Densities (Ah dm^{-2})									
			0.5	1	1.5	2	3	4	5	6	8	10
2	0.18	0.17	20	10	6.8	5.1	3.4	2.6	2.0	1.7	1.3	1
4	0.36	0.34	41	20	14	10	6.8	5.1	4.1	3.4	2.6	2
6	0.53	0.51	61	31	20	15	10	7.7	6.1	5.1	3.8	3.1
8	0.71	0.68	82	41	27	20	13	10	8.2	6.8	5.1	4.1
10	0.89	0.85	100	51	34	26	17	13	10	8.5	6.4	5.1
12	1.1	1.0	120	61	41	31	20	15	12	10	7.7	6.1
14	1.2	1.2	140	71	48	36	24	18	14	12	8.9	7.1
16	1.4	1.4	160	82	54	41	27	20	16	14	10	8.2
18	1.6	1.5	180	92	61	46	31	23	18	15	11	9.2
20	1.8	1.7	200	100	68	51	34	26	20	17	13	10
40	3.6	3.4	410	200	140	100	68	51	41	34	26	20

2.11.2 Functional Electroplating and Deposit Properties

Electrodeposited nickel coatings are applied in functional applications to modify or improve corrosion resistance, hardness, wear, magnetic, and other properties.

The main constituents in Watts's solutions affect the properties of electrodeposited nickel. Nickel sulfate improves conductivity and metal distribution and determines the limiting cathode current density for producing sound nickel deposits. Nickel chloride improves anode corrosion but also increases conductivity, throwing power, and uniformity of coating thickness distribution. In addition chlorides increase the internal stress of the deposits, and they tend to refine grain size and minimize formation of nodules and trees. Boric acid is added for buffering purposes and affects the appearance of the deposits. Deposits may be cracked and burnt at low boric acid concentrations. Anionic wetting agents or surfactants that lower the surface tension of the plating solution so that air and hydrogen bubbles do not cling to the parts being plated are almost always added to control pitting and, by eliminating porosity, have an indirect effect on corrosion performance.

Table 2.3 Nickel Plating Solutions (Mordechay Schlesinger, 2010).

	Electrolyte Composition(gL^{-1})		
Solution	**Watts Nickel**	**Nickel Sulfamate**	**Basic Semibright Bath**
Nickel sulfate, $NiSO_4.6H_2O$	225-400	-	300
Nickel Sulfamate,$Ni(SO_3NH_2)_2$	-	30-45	-
Nickel choloride, $NiCl_2.6H_2O$	30-60	300-450	35
Boric acid,H_3BO_3	30-45	0-30	45
		Operating Condition	
Temperature(°C)	44-46	32-60	54
Agitation	Air or mechanical	Air or mechanical	Air or mechanical
Cathode current density($A\ dm^{-2}$)	3-11	0.5-30	3-10
Anodes	Nickel	Nickel	Nickel
PH	2-4.5	3.5-5.0	3.5-4.5
		Mechanical Properties	
Tensile strength(MPa)	345-435	415-610	-
Elongation (%)	10-30	5-30	8-20
Vickers hardness(100 g load)	130-200	170-230	300-400
Internal stress(MPa)	125-185	0-55	35-150

Operating conditions, such as pH, temperature, current density and chloride content, affect the properties of deposits from Watts solutions. Table 2.3 shows the properties of nickel Plating Solutions.

2.12 Summary and Conclusion

Several challenges should be met before the lead-based solders are utterly replaced by the lead-free solders in the microelectronic packaging. The trend of miniaturization and functional density enhancement requires much smaller solder joints with a fine pitch interconnection. These ultra-fine solder joints lead to high homologous temperature during services which may lead to coarsening of the microstructure at the solder/substrate interface. The key issue to ensure a fine and uniform solder joint microstructure is to slow down the interfacial reactions between the solder and substrate.

Numerous solders have been studied by researchers worldwide. Most is focused on the bulk microstructure and mechanical properties with and without the addition of additives. Some research concentrate on the addition of alloying elements and nanoparticles to the lead-free solder. It was found from the previous research that addition of Fe, Co, Ni as an alloying element to the solder increases the intermetallic compound formation at the solder/substrate interface. Beside, nanoparticles of Co and Ni also show a similar trend of increasing the intermetallic compound thickness. Addition of inert nanoparticles such as TiO_2, Al_2O_3, CNTs focus only the bulk microstructure and mechanical properties of the solder. No research has been done on the interfacial IMC with the addition of inert metallic nanoparticles.

Previous studies showed that the addition of Mo nanoparticles to SAC solder causes a decrease in the thickness and diameter of interfacial Cu_6Sn_5 scallops (Haseeb et al., 2012). In this research the interaction between SAC solder in the presence of Mo Nanoparticle and electroplated cu substrate with Ni is studied.

Chapter 3: Methodology

3.1 Raw Materials and Characterization

In this study, molybdenum nanoparticle (99.8% trace metal basis) was used as a reinforcing material with the Sn-3.8Ag-0.7Cu (SAC) solder paste (Indium Corporation of America). The particle size of the SAC solder paste was investigated from scanning electron microscopy (SEM, Philips XL-40) image. First by using propanol, flux from the solder paste was removed. Then a small amount of solder sample was taken in a sample holder and dried at 100ºC for one hour in an oven. Finally the dried solder was analyzed under SEM.

The morphology and size of the Mo nanoparticles were determined by using a Philips CM200 transmission electron microscopy (TEM). Firstly, a small amount of Mo nanoparticles were dispersed into distilled water onto a carbon film supported by copper grids. The grain size measurement and phase analysis of Mo nanoparticles was conducted by X-Ray diffractometer (XRD). The nanoparticles were exposed to CuK_α (λ=0.15406 nm) radiation with a scanning speed of 2º/min in the 10-80º diffraction range with a step size of 0.05º.

3.2 Sample Preparation and Treatment

3.2.1 Preparation of Copper Substrate with Electroplated Ni

Commercial polycrystalline copper sheets (30mm×30mm×0.3mm) were used for the preparing of the solder joint. Prior to electroplating, the sheets were cleaned by detergent followed by dipping in 10 vol%$\mathrm{H_2}SO_4$ remove oxide after that the sheets were rinsed thoroughly in distilled water followed by cleaning with acetone. After the cleaning, Watts's Nickel plating bath was used to electroplate Ni on copper substrate. The plating solutions with plating parameters are shown in Table 3.1.

Table 3.1 Plating solution and parameters for the deposition of Ni on Cu substrate (Mordechay Schlesinger, 2010).

Type	**Composition(g L^{-1})**	**pH**	**Temperature (°C)**	**Cathode current density (mA/cm^2)**
Watts nickel	Nickel sulphate $NiSO_4.6H_2O$,300 Boric acidH_3BO_3,35 Nickel chloride $NiCl_2.6H_2O$,45	3.5	55	50

The condition that is mentioned in Table3.2 is used to electrodeposit Ni with10 μm thickness on Cu substrate.

Table 3.2 Nickel electroplating data(Mordechay Schlesinger, 2010)

Deposit nickel (μm)	**Weight per unit area (gdm^{-2})**	**Ampere hours per unit $(A\text{h } dm^{-2})$**	**Time(min) to obtain deposit with $50\ mA/cm^2$current density**
10	0.89	0.85	10

3.2.2 Preparation of Composite Solder Paste and Nanoparticles Distribution

Mo nanoparticles were mixed manually with Sn-3.8Ag-0.7Cu (SAC) solder paste for nominal compositions of 1and 3 wt%. A homogeneous paste composition was obtained by 30 min mixing. The distribution of Mo nanoparticles in the SAC solder paste was found by taking small amount composite paste to a SEM sample holder. Then it was placed in an oven and heated at 100ºC for one hour to dry the paste composition. After that, the dry composite paste was analyzed by high resolution field emission scanning electron microscopy (Zeiss Ultra-60 FESEM) and energy-dispersive X-ray spectroscopy (EDX, EDAX-Genesis Utilities) to check the distribution of Mo nanoparticles into the SAC solder.

3.2.3 Preparation of Reflowed Samples

Prepared copper substrate with electroplated Ni layer is rinsed thoroughly in distilled water and finally cleaned with acetone. After the surface preparation the composite solder paste was placed on the copper substrate through a mask having an opening diameter of 6.5mm and 1.24mm thickness (JIS Z3198-3, 2003). Then the composite solder paste was reflowed on a hot plate at 250ºC for 45 s.

3.2.4 Multiple Reflow

After first reflow one set of samples were reflowed again in a reflow oven (Forced convection, FT02) for six times at 250ºC for 45s. After reflow, the solders were cleaned with acetone to remove the flux residue. The multiple reflowed samples were also cross sectioned, mounted in epoxy and polished by employing the standard metallographic techniques. The cross-sectional view of the interfacial IMC was observed by backscattered electron detector under a field emission scanning electron microscope (FESEM). The elemental analysis was carried out by using energy dispersive X-ray spectroscopy (EDX). To expose the top surface of the intermetallic compound, samples were chemically etched for 24h as it is mentioned previously. In this case also the microstructure was observed by high resolution field emission SEM (Zeiss Ultra-60 FESEM). The elemental analysis was carried out by energy-dispersive X-ray spectroscopy (EDX, EDAX-Genesis Utilities).

3.3 Characterization of Solder

3.3.1 Differential Scanning Calorimetry Measurement of Solder Paste

Differential scanning calorimetry (DSC, Mettler DSC 820, Switzerland) measurements were conducted to find out the melting temperatures of the composite solder pastes.

Samples were weighted by a microbalance (~10-15mg). Then the samples were placed on a 70µl platinum crucible inside the DSC furnace and heated to 250ºC at a heating rate of 10ºC/min. The onset temperature in the DSC curve was taken as the melting point of the solders.

3.3.2 Inductively coupled-Optical Emission Spectrometer

The solder samples were chemically analyzed by inductively coupled-Optical Emission Spectrometer (ICP-OES, Perkin Elmer Optima 2000 DV) to find out the actual amount of molybdenum content in the solder. After reflow, the flux residue on top of the solder matrix was removed by hexane. The solders were scratched out using tweezers. After that 0.5g of flux residue and solders were digested in 5 ml concentrated hydrochloric acid (HCl) separately and then diluted to 100 ml deionized water. The calibration standard solution of Mo (Cat No. 1.70227.0500, Merck) were prepared from the 1000 ppm stock solution. Each calibration curve was created using three standard concentration curves (2, 4 and 6 ppm). The concentration of Mo inside the solder and flux was indicated by the intensity of the emission.

3.3.3 Spreading Rate and Wetting Angle

The ability of the molten solder to spread over the substrate is used to measure the wetting behavior. After first reflow, twelve samples were utilized to calculate the spread rate according to the Japanese Industrial Standard (JIS Z3198-3, 2003). According to the Japanese Industrial Standard, the spread rate was calculated by the following equation

$$S_R = \frac{D - H}{D} \times 100 \tag{3.1}$$

$$D = 1.24V^{1/3} \tag{3.1}$$

Where, SR = Spread rate (%), H = Height of the spread solder (mm), D = Diameter when the solder used for a test is considered as a ball (mm) and V = Mass/density of the solder sample used for the test = 7.5 gm/cm^3.

After calculating the spreading rate, the solder samples were cross sectioned, mounted in epoxy and polished up to 0.02 μm finish by employing standard metallographic technique for measuring the wetting angle by optical microscope.

Chapter 4: Results and Discussion

4.1 Characterization of Raw Materials

4.1.1 Morphological Characterization and Particle Sizes of Solder Paste

Mo nanoparticles used in this study were characterized in an earlier study (Arafat, 2012). Figure 4.1 shows the scanning electron microscopy (SEM) image of Sn-3.8Ag-0.7Cu (SAC) solder balls in the solder paste. Flux was removed from the SAC solder paste by dissolving it in propanol. It was seen that shape of the SAC solder balls was spherical with a small variation in diameter. The average diameter of the solder balls calculated from Figure 4.1 was 34±6µm.

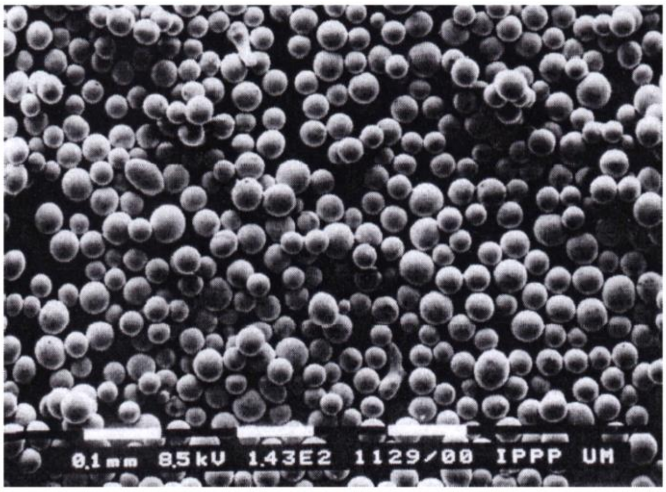

Figure 4.1 SEM image of SAC solder powder (Flux has been removed) (Arafat, 2012).

4.1.2 TEM of Mo Nanoparticles

Figure 4.2 shows a transmission electron microscopy (TEM) micrograph and the particle size distribution of Mo nanoparticles. More than 250 particles were used for calculating particle size distribution. It is found from the distribution that the size of the most particles is in between 20-100 nm, although some particles are as big as 200 nm.

But the frequency of the particles having size more than 200 nm is quite low. The weighted average of the size distribution shows that the average size of Mo nanoparticles is 70 nm.

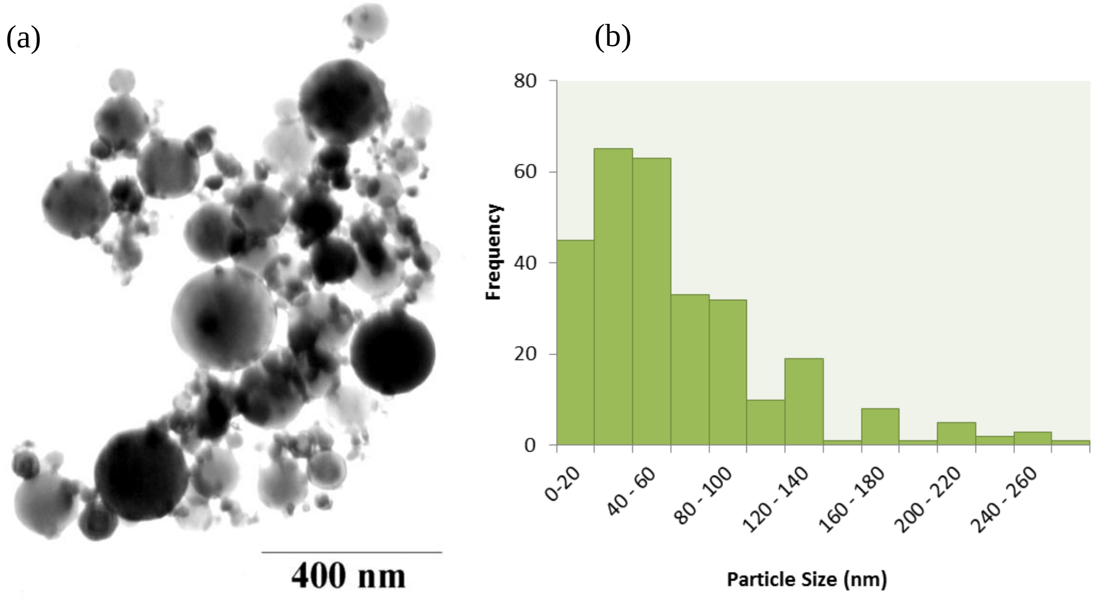

Figure 4.2 (a) TEM micrograph of the Mo Nano-particles, (b) Histogram of particle size (Arafat, 2012).

4.1.3 X-Ray Diffraction of Mo Nanoparticles

The XRD pattern of the Mo nanoparticles is demonstrated in Figure 4.3. Three strong peaks at 40.509º, 58.599º and 73.660º clearly indicates the presence of (110), (200) and (211) crystal plane in Mo nanoparticles respectively. It may be noted that no oxide peak was observed from the XRD pattern. The grain size of Mo nanoparticles was calculated by using the Scherrer’s Equation. 4.1.

$$L = \frac{k\lambda}{\beta \cos \theta} \qquad 4.1)$$

Where K is the shape factor, λ is the X-ray wavelength, β is the line broadening at half the maximum intensity (FWHM) in radians, and θ is the Bragg angle. L is the mean size of the ordered (crystalline) domains, which may be smaller or equal to the grain size.

The Scherrer's equation was corrected by assuming the parameter β as a Gaussian function for the diffraction peaks and instrumental broadening. The average grain size of Mo nanoparticle was found around 40 nm.

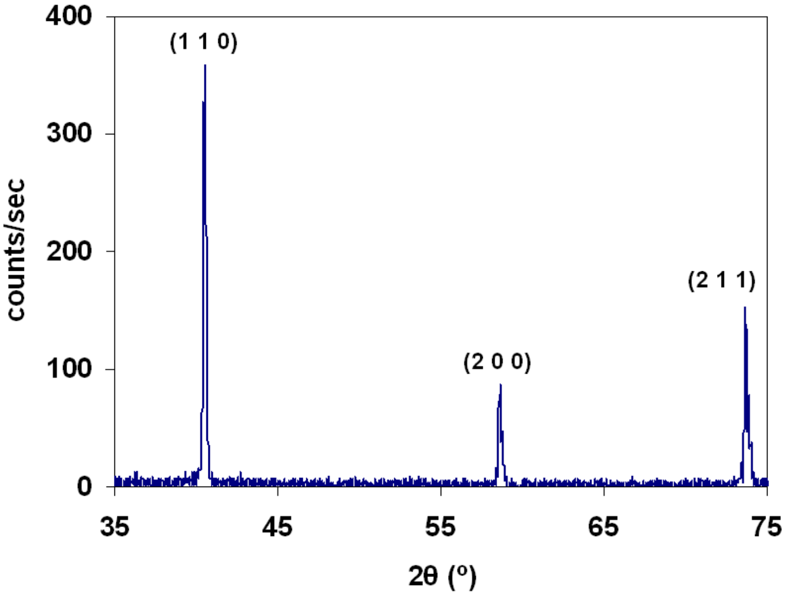

Figure 4.3 X-Ray diffraction (XRD) pattern of Mo nanoparticles (Arafat, 2011).

4.2 Distribution of Mo Nanoparticles in the SAC Solder Paste

The spatial distribution and elemental mapping of the solder paste nominally containing 2 wt% Mo is shown in Figure 4.4. Figure 4.4(a) shows an overall view of the paste at a lower magnification. It is seen in Figure 4.4(a) that tiny Mo nanoparticles adhere to the surface of large SAC solder balls. Mo nanoparticles were also seen in the flux situated at the crevices between SAC balls. High magnification images provide clean views of both SAC ball surface (Figure 4.4c) and flux (Figure 4.4d). It is observed that Mo nanoparticles are fairly well distributed in the paste.

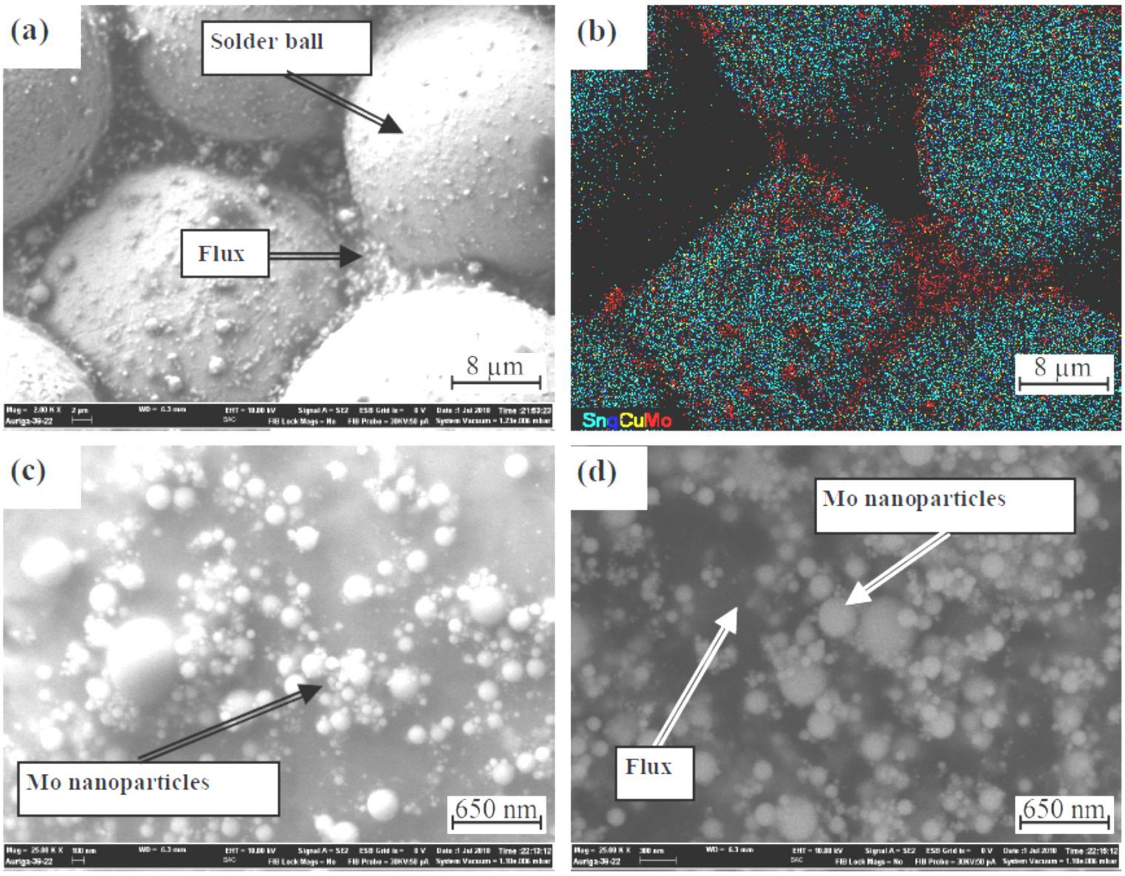

Figure 4.4FESEM images of solder paste after blending, nominally containing 2 wt% of Mo nanoparticles (a) distribution of Mo nanoparticles into the solder paste, (b) elemental mapping of the composite paste showing Mo (red), Sn (cyan), Ag (blue), and Cu (yellow), (c) high resolution image focused on the solder ball surface and (d) high resolution image focused on the flux (Arafat et al., 2011).

4.3 Chemical Analysis of the Reflowed Samples

Upon reflow, the solder balls melted, coalesced and formed the solder joint. The flux residue stays on the surface of the solder joint. In order to find out how much Mo nanoparticles is retained in the solidified solder, the latter was chemically analyzed by inductive coupled plasma-optical emission spectroscopy ICP-OES. The actual Mo content of the solder is shown in the Table 4.1. For the nominal addition of 1 and 3 wt% of Mo nanoparticles into the solder paste, the actual content in the solder is found to be only 0.04 and 0.14 wt% of Mo respectively. The rest of the Mo enters in the flux residue (Arafat et al., 2011). Hereafter, solders actually containing 0.04 and 0.14 wt % Mo will be designated as (SAC + 0.04 n-Mo) and (SAC + 0.14 n-Mo) respectively with n referring to nanoparticles.

Table 4.1 Molybdenum content of solders analyzed by ICP-OES after reflow.

Nominal Mo Content, wt %	Actual Mo content in the solder, wt %	Actual Mo content in the flux, wt %
1.0	0.04	5.40
3.0	0.14	-

It may be noted that the solder paste consists of a flux in which SAC solder balls were dispersed. After the addition and mixing of nanoparticles, the Mo nanoparticles also dispersed within in the flux remaining in between the SAC balls (Figure 4.4). During reflow process, a fraction of the nanoparticles enters the molten pool of solder and eventually got trapped inside the solidified solder mass. The rest stays with the flux residue. Similar result was obtained for Co nanoparticles (Arafat et al., 2011).However, in the case of Co nanoparticles, the fraction of nanoparticles retained in the solder was higher. The incorporation of nanoparticles into solder will mainly depend on the interactions between nanoparticles and the solder. It has been suggested that a reinforcing particle can be pushed (rejected), engulfed or entrapped at the particle-liquid metal interface depending upon the interaction mechanisms(Dhindaw, 1999, Wilde and Perepezko, 2000). The incorporation of a lower amount of Mo in SAC suggests that Mo nanoparticles experiences rejection by the liquid SAC interface to a greater extent. Poor wetting of Mo and SAC could be a reason for higher rejection. In spite of the rejection, the amount of Mo nanoparticles still retained in the solder has definite influence on interfacial IMC growth characteristics as will be discussed later. This simple paste mixing method to incorporate nanoparticles into the solder is gaining increasing attention by the researchers nowadays. Reported results on sample prepared by paste mixing method also show that enough nanoparticles can be incorporated to the solder to enhance its properties(Tai et al., 2005). On the other hand this method can be used in the conventional reflow process using the existing industrial infrastructure(Zerrer et al., 2008).

4.4 Spreading Rate and Wetting Angle

Figure 4.5 shows the spreading rate and wetting angle of the Mo added nanocomposite solder as a function of nanoparticles content. The spreading rate drops from 74.22%to 66.34% for (SAC + 0.14 n-Mo) solder (Figure 4.5 a). On the other hand the wetting angle increases from 17.3º to 28.9º to the (SAC + 0.14 n- Mo) (Figure 4.5.b).

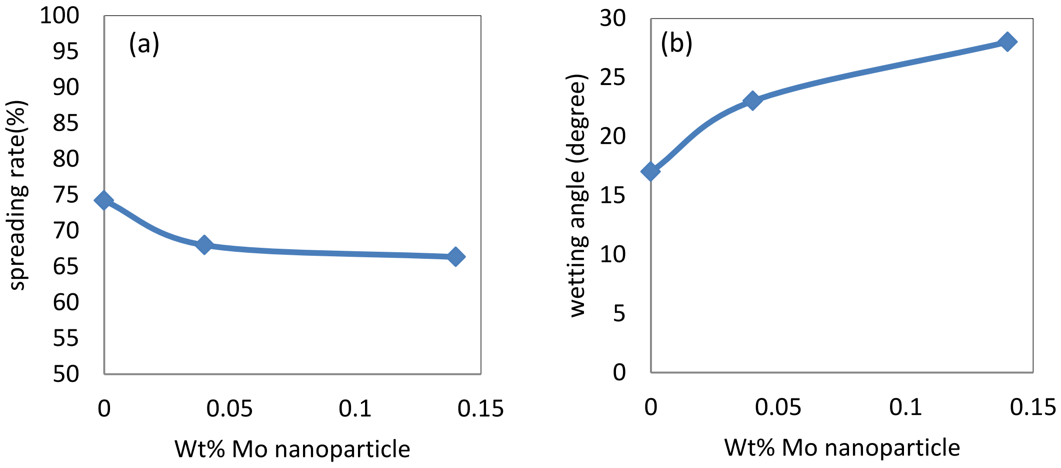

Figure 4.5 (a) Spread rate and (b) wetting angle as a function of wt % of Mo nanoparticles.

Actually, spreading rate and wetting angle are used to measure the solderability of the composite paste. For good metallurgical bond between solder and substrate, the spreadability and wettability should be in acceptable range. It is generally agreed that higher spreading rate with a lower wetting angle is desired during reflow. With increasing Mo nanoparticles up to 0.1 wt % into the SAC solder paste the spreading rate decreases from 74.22%to 66.34% but the wetting angle increases from 17.3º to 28.9º However Mo nanoparticles-added SAC solder shows a considerable solderability comparing the SAC and Sn-Pb solder(Wang et al., 2008a). Reported results of wetting angle by wetting balance technique for Sn-Pb solder on Cu substrate was found 20º

(Wang et al., 2008a). The possible reason for decreasing spreading rate could be due to the increase of melt viscosity for addition of nanoparticles into solder paste. Increased amount of nanoparticles inhibits the molten composite solder to flow on the substrate(Nai et al., 2006). Inhibition to flow of the composite melt on the substrate is believed to lead higher wetting angle compare with SAC solder.

Arafat (2012) showed that the spreading rate of SAC+0.14n-Mo on Cu substrate decreased from 79.8 to 76.8% and wetting angle increased from 17.8° to 28.8°. In comparison it is seen that for Ni substrate, the spreading rate decreased from 74.22%to 66.34% and wetting angle increased from 17.3° to 28.9° upon the addition of 0.14 % Mo nanoparticle (Figure 4.5).

4.5 Analysis of Electroplated Ni on Copper Substrate

The FESEM image in Figure 4.6 illustrates the thickness of electroplated Ni on copper substrate. On the basis of electroplating condition mentioned in Tables 3.1 and 3.2, theoretically the thickness should be 10µm. EDX confirms that dark contrast layer with homogenous uniform morphology is Ni. The measurement of this layer on all samples show that the avarage Ni thickness is 6.5±0.5µm. The lower thickness would be due to lower current efficiency of Ni plating.

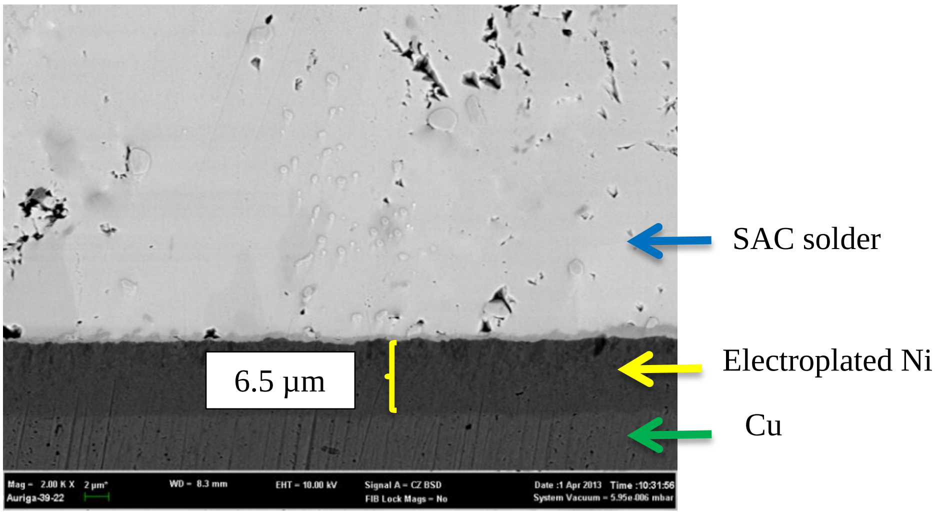

Figure 4.6 SAC on copper substrate with a top layer of electroplated Ni.

4.6 IMC Morphology on Ni and Cu Substrate

FESEM results show the IMC morphology of SAC and SAC+ 0.14 n-Mo on Cu and Ni substrate in Figures 4.7. The IMC at the interface between SAC and Cu substrate has scallop shape, in Figure 4.7a and 4.7b but 0.14 n-Mo in 4.7b decrease the size of scallop. It is shown in Figure 4.7b that there are existed 2 layers of IMC (points Y and Z) at interface and one IMC inside the bulk of the SAC solder (point X). Figure 4.7c and 4.7d show flat shape IMC at the Ni substrate, adding 0.14 n-Mo (4.7d) decreased the thickness. The Figure 4.7c shows the one layer of IMC at interface (point γ) and 2 kind of IMC inside the bulk of SAC solder (points α and β).

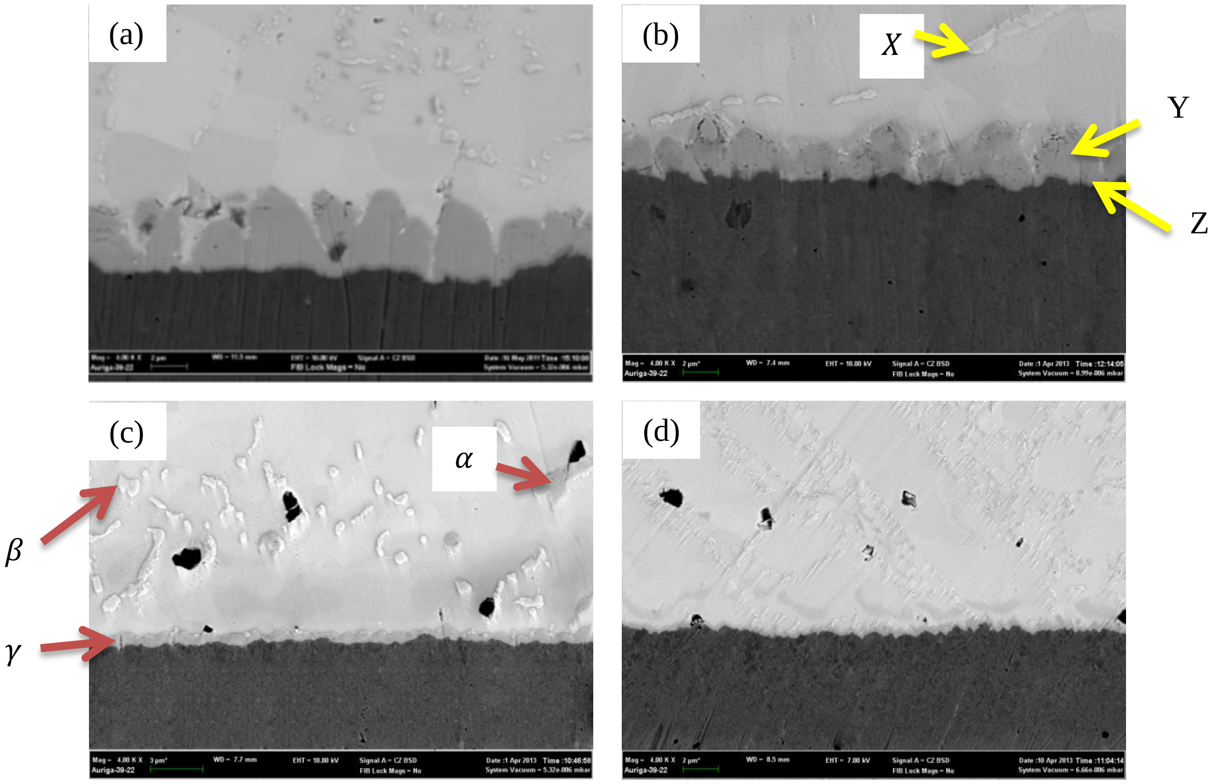

Figure 4.7 IMC morphology of (a) SAC on Cu substrate after 1st reflow, (b) SAC+0.14 n-Mo on cu substrate after 1st reflow (c)SAC on Ni substrate after 1st reflow (d) SAC +0.14 n-Mo on Ni substrate after 1st reflow.

Figure 4.8 shows the EDX at the interface between SAC+0.14 n-Mo on Cu substrate, it reveals that the IMC at point Y is Cu_6Sn_5 . Figure 4.9 demonstrates Cu_6Sn_5 and Cu_3sn IMC on the copper substrate. The EDX result in figure 4.10 shows the compound at point γ ($(\mathrm{Cu}_{1-x}, \mathrm{Ni}_x)_6\mathrm{Sn}_5$), and the Figure 4.11 illustrate the intermetallic compound at interface and in the bulk of the solder on Ni substrate. On all samples, the composition of $(\mathrm{Cu}_{1-x}, \mathrm{Ni}_x)_6\mathrm{Sn}_5$, Ag_3Sn and $\mathrm{Cu}_6\mathrm{Sn}_5$ was confirmed by EDX. Mo nanoparticle was not detected in cross sectional view but detected in top view (Arafat, 2012).

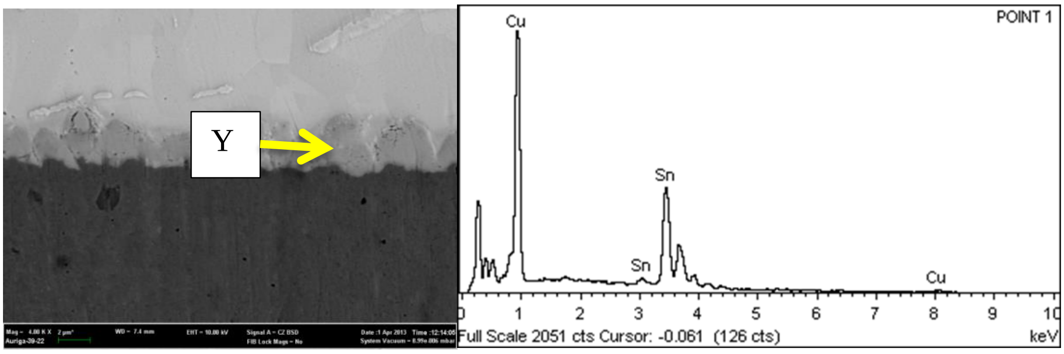

Figure 4.8 EDX result at the interface between Cu substrate and SAC solder (point Y).

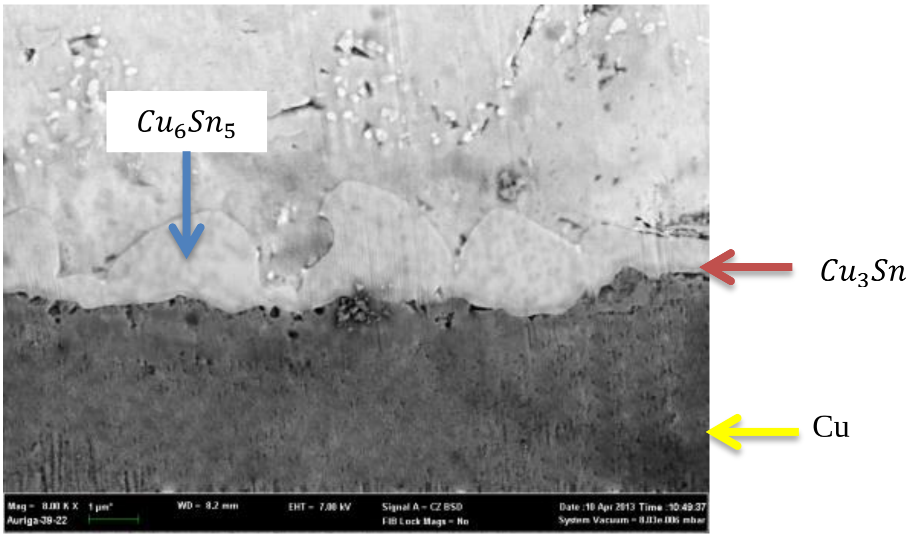

Figure 4.9SAC+ 0.14 n-Mo after 6th reflow on copper substrate.

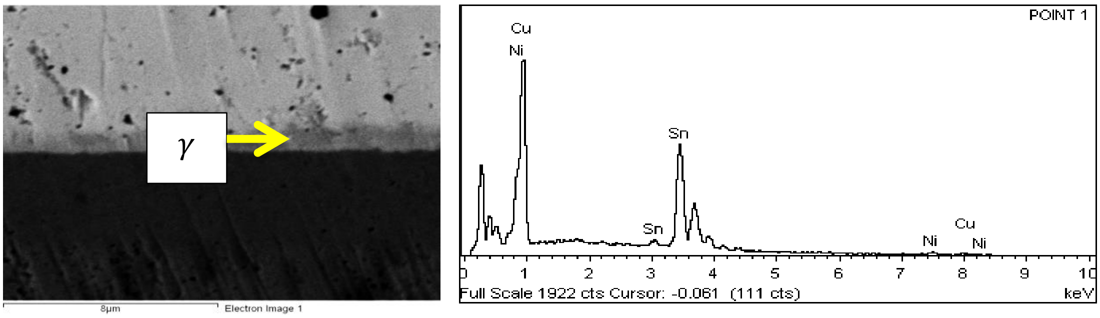

Figure 4.10 EDX result at the interface between Ni layer and SAC solder (point$\boldsymbol{\gamma}$).

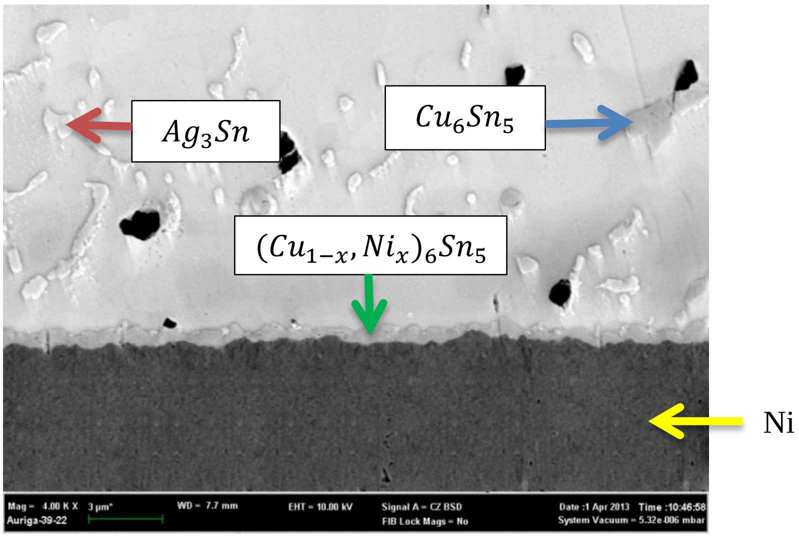

Figure 4.11 Intermetallic compound between the SAC solder and the Ni substrate.

4.7 Effect of Mo Nanoparticles on IMC

Figure 4.12 shows the cross sectional backscattered electron micrographs of SAC, (SAC + 0.04 n-Mo) and (SAC + 0.14 n-Mo) after first and six reflow on Ni substrate. Formation of IMC between the solder and Ni substrate is clearly visible.

A comparison between Figures 4.12a, 4.12b and 4.12c show that the addition of Mo nanoparticles results in a decrease in overall IMC thickness after first reflow. The effect of Mo nanoparticles is evident after six times reflow as well (Figures 4.12d, 4.12e and 4.12f). No molybdenum could be detected inside the $(Cu,Ni)_6Sn_5$ IMC by EDX analysis for both first time and six times reflow.

The thickness of the interfacial IMC increases with an increase in the number of reflow for both SAC and Mo nanoparticle added SAC solder. But the thickness of the interfacial IMC is lower, first the Ni layer on copper in compare to the Cu substrate decrease the IMC thickness because the Ni works as the barrier and prevent Cu to diffuse inside the IMC and increase its thickness, second the Mo nanoparticles-added solder compared with the SAC solder can decrease the IMC thickness too .The IMC thickness in SAC+0.14n-Mo on copper after first reflow is around 2.02µm and Ni substrate is 0.51µm, it is clearly shows the effect of Ni substrate to decrease the IMC thickness.

Figure 4.13 shows the effect of different percent of Mo Nanoparticle on IMC thickness on SAC solder after 1st reflow and 6th reflow on Ni substrate. Lower IMC thickness is observed for all Mo nanoparticles-added samples.

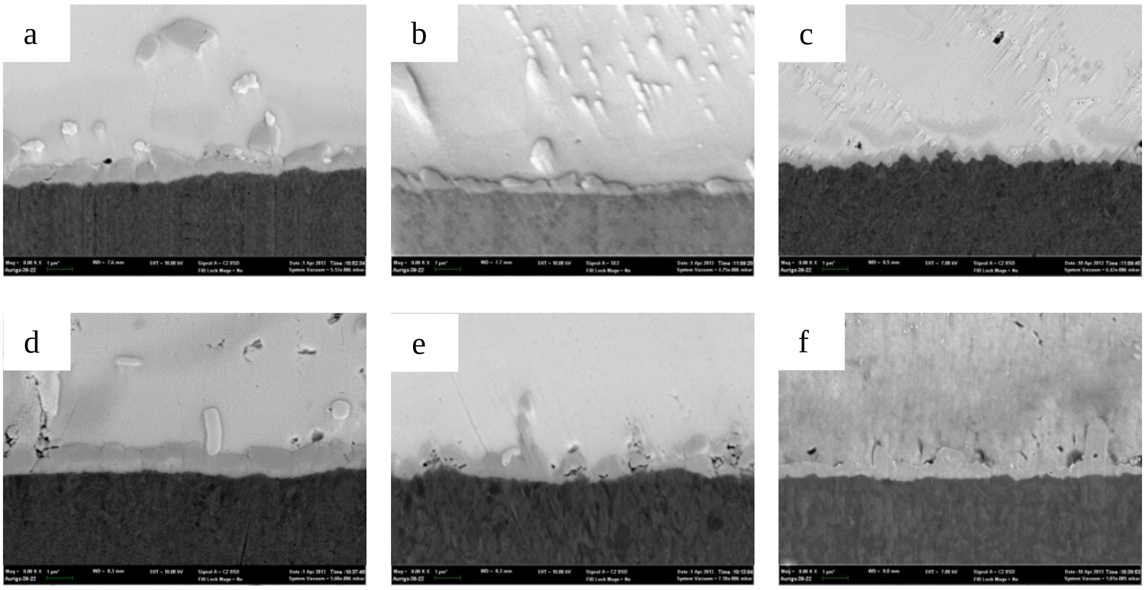

Figure 4.12Backscattered electron micrographs of the cross sectional view (a) SAC after first times reflow, (b) (SAC + 0.04 n-Mo) after first times reflow, (c) (SAC + 0.14 n-Mo) after first times reflow ,(d) SAC after six times reflow and (e) (SAC + 0.04 n-Mo) after six times reflow(f) (SAC + 0.14 n-Mo) after six times reflow (All has same magnification of 4.00 KX).

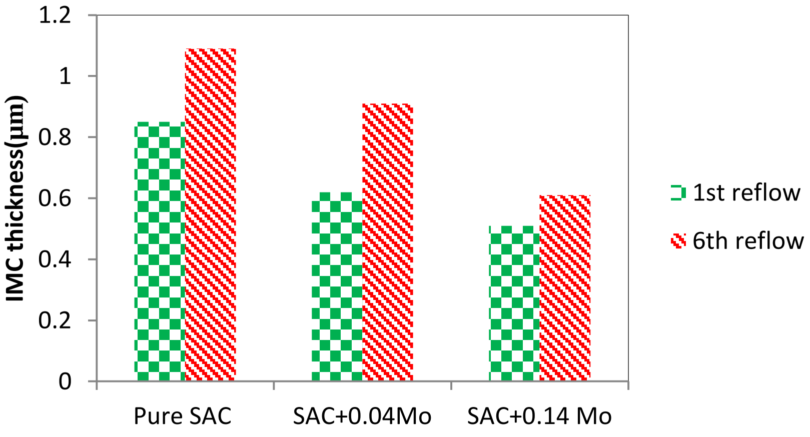

Figure 4.13 Effect of Mo nanoparticles on the IMC thickness.

4.7.1 State of Mo Nanoparticles during Reflow

The exact mechanism(s) of the Mo nanoparticles to suppress the growth of interfacial IMC thickness and scallop diameter is not obvious. However, several cases are speculated. In one case, nanoparticles may remain as discrete, unaltered particles during reflow. On the other one, they can be completely consumed in some reaction(s) or through dissolution within the molten solder. Actual alteration that the nanoparticles may undergo will depend on a number of factors, including their melting point and chemical interaction(s) with the solder. Molybdenum has a relatively high melting point (2623ºC) compared with the reflow temperature (250ºC) used in this study. So, under the present experimental condition, Mo nanoparticles are not expected to physically melt during reflow. Referring to the Mo- Sn phase diagram, Mo has negligible solubility in Sn. The phase diagram shows that as many as three IMCs e.g., Mo_3Sn, Mo_2Sn_3/Mo_3Sn_2, and $MoSn_2$ can exist in the Mo-Sn system(Brewer and Lamoreaux, 1980). But no evidence of Mo-Sn compound formation was found on Mo nanoparticles by EDX. It may be noted that Mo does not form any compound with Cu and Ag at 250ºC, and has no solubility in these elements (Baren, 1990, Subramanian and Laughlin, 1990).

4.7.2 Suggested Mechanism for Retardation of IMC Growth by Mo Nanoparticles

When Mo nanoparticles are mixed with SAC solder paste and reflowed at 250ºC, they remain as stable solid particles. The nanoparticles do not particularly undergo any kind of chemical reactions or dissolution. So the retardation of IMC growth and scallop diameter are solely due to the particle effect of Mo nanoparticles. There can be three possibilities through which Mo nanoparticles can lower the thickness and reduce the diameter of IMC scallop:

a. Mo nanoparticles can act as heterogeneous nucleation sites for the formation of $(Cu,Ni)_6Sn_5$ nucleus. This can increase the density of nucleation of $(Cu,Ni)_6Sn_5$ grains,

b. Mo nanoparticles may have pinning effect on the growing front of $(Cu,Ni)_6Sn_5$ scallops, and

c. Both (a) and (b).

For a particle to act as a heterogeneous nucleation site, the interfacial energy between the liquid and solid particles should be low. In other words, the wetting angle of the liquid at the solid surface should be low. No data on the interfacial energy and wetting angle between liquid $(Cu,Ni)_6Sn_5$ and Mo is available in the literature. If the Mo nanoparticles act as heterogeneous nucleation sites, it is likely that the nanoparticles could be formed as inclusions in the $(Cu,Ni)_6Sn_5$ scallops. Extensive examination of multiple samples on cross-section under high resolution FESEM could not identify any such inclusion. These lead on to suggest that Mo nanoparticles are unlikely to act as heterogeneous nucleation sites. It is therefore believed that the influence of Mo nanoparticles on the $(Cu,Ni)_6Sn_5$ layer is due to their effect on the growth process.

Previous studies show that higher percentage of Mo was found on the IMC surface (3-3.5 wt %) compared with the average Mo content of the solder. Therefore their presence on the IMC surface, Mo nanoparticles are believed to have a retarding effect on the IMC growth (Arafat, 2011).

Molybdenum being a refractory metal with high melting point and low reactivity remains stable during reflow. These particles do not undergo any detectable alteration during reflow. It is therefore suggested that Mo nanoparticles exert their influence on the interfacial IMC growth as discrete particles.

Chapter 5: Conclusion and Recommendation

5.1 Conclusions

In this research, effects of Mo nanoparticles on Sn-3.8Ag-0.7Cu (SAC) solder on Ni substrate were investigated. The results obtained from this research work have lead to the following conclusions:

- During reflow only a fraction of Mo nanoparticles is incorporated into the solder. The rest of the nanoparticles stay inside the flux residue. The incorporation of a lower amount of Mo in SAC suggests that Mo nanoparticles experiences rejection by the liquid SAC interface. Poor wetting of SAC on Mo could be a possible reason for this rejection.
- The addition of Mo nanoparticles into SAC solder decreases the spreading rate and increases the wetting angle. For the addition of 0.14 wt % of Mo nanoparticles into the SAC solder the spreading rate drops from 74.22 to 66.34% and wetting angle increased from 17.3º to 28.4º.
- The addition of Mo nanoparticles to SAC solder causes a decrease in the thickness of interfacial $(Cu,Ni)_6Sn_5$ with planar morphology during multiple reflow. During reflow, Mo nanoparticles exert their influence on the interfacial IMC through discrete particle effect by preferentially absorbing at the grain boundaries of interfacial IMC. This mechanism suppresses the growth of $(Cu,Ni)_6Sn_5$ IMC and produces thinner IMC layer during reflow. Mo nanoparticles are suggested to have more influence on IMC growth rather than nucleation.

5.2 Recommendation for Future Work

- The strength of interfacial IMC is important to determine the reliability of the solder. Investigating the strengh of the solder joint by nanoindentation test is suggested for the future study.
- In this present experimental work nanocomposite solders were reflowed on Ni substrate (Ni/Cu). It is recommended for the future work to reflow the nanocomposite solders on different substrates such as ball grid array (BGA), flip chip (FC) with different surface finishes such as electroless Ni(P)/Au, electrolytic Ni/Au, Al/Ni(V)/Cu, Zn(Mo)/Cu etc. These processing techniques are more close to industrial practices in the microelectronics industries.
- Investigations on the mechanism through which nanoparticles influence the interfacial IMC can be carried out by high resolution transmission electron microscopy(TEM).
- Various processing routes for the incorporation of different nanoparticles inside the solder matrix can be explored.

References

Abtew, M. & Selvaduray, G. 2000. Lead-free Solders in Microelectronics. *Materials Science and Engineering: R: Reports,* 27**,** 95-141.

Amagai, M. 2008. A study of nanoparticles in Sn–Ag based lead free solders. *Microelectronics Reliability,* 48**,** 1-16.

Arafat, M., Haseeb, A. & Johan, M. R. 2011. Interfacial reaction and dissolution behavior of Cu substrate in molten Sn-3.8 Ag-0.7 Cu in the presence of Mo nanoparticles. *International Journal of Soldering and surface mount technology,* 30**,** 17-31.

Arafat, M. M. 2012. Effects of molybdenum nanoparticles on lead-free tin-based solder. Universiti Malaya.

Baren, M. R. 1990. The Ag-Mo (Silver-Molybdenum) system. *Bulletin of Alloy Phase Diagrams,* 11**,** 548-549.

Bath, J. 2010. *Lead-Free Soldering,* New York, USA, Springer.

Boettinger, W. J., Johnson, C. E., Bendersky, L. A., Moon, K. W., Williams, M. E. & Stafford, G. R. 2005. Whisker and Hillock formation on Sn, Sn–Cu and Sn–Pb electrodeposits. *Acta Materialia,* 53**,** 5033-5050.

Brewer, L. & Lamoreaux, R. H. 1980. The Mo-SN (Molybdenum-Tin) system. *Bulletin of Alloy Phase Diagrams,* 1**,** 96-97.

Chandra Rao, B. S. S., Weng, J., Shen, L., Lee, T. K. & Zeng, K. Y. 2010. Morphology and mechanical properties of intermetallic compounds in SnAgCu solder joints. *Microelectronic Engineering,* 87**,** 2416-2422.

Cheng, F., Gao, F., Nishikawa, H. & Takemoto, T. 2009. Interaction behavior between the additives and Sn in Sn–3.0 Ag–0.5 Cu-based solder alloys and the relevant joint solderability. *Journal of Alloys and Compounds,* 472**,** 530-534.

Chidambaram, V., Hattel, J. & Hald, J. 2010. Design of lead-free candidate alloys for high-temperature soldering based on the Au–Sn system. *Materials & Design,* 31**,** 4638-4645.

Das, S., Sharif, A., Chan, Y., Wong, N. & Yung, W. 2009. Effect of Ag micro-particles content on the mechanical strength of the interface formed between Sn–Zn binary solder and Au/Ni/Cu bond pads. *Microelectronic Engineering,* 86**,** 2086-2093.

De Gennes, P. G. 1985. Wetting: statics and dynamics. *Reviews of Modern Physics,* 57**,** 827-863.

Dhindaw, B. K. 1999. Interfacial energy issues in ceramic particulate reinforced metal matrix composites. *Bulletin of Materials Science,* 22**,** 665-669.

DiBari, G. A. 1996. Nickel electroplating applications & trends. *Plating and surface finishing,* 83**,** 10-14.

Felton, L., Raeder, C. & Knorr, D. 1993. The properties of tin-bismuth alloy solders. *JOM,* 45**,** 28-32.

Franke, P. & Neuschütz, D. 2005. Cu-Sn. *In:* Franke, P. & Neuschütz, D. (eds.) *Binary systems. Part 3: Binary Systems from Cs-K to Mg-Zr.* Springer Berlin Heidelberg.

Gain, A. K., Chan, Y. C. & Yung, W. K. C. 2011. Microstructure, thermal analysis and hardness of a Sn–Ag–Cu–1wt% nano-TiO2 composite solder on flexible ball grid array substrates. *Microelectronics Reliability,* 51**,** 975-984.

Ganesan, S. & Pecht, M. G. 2006. *Lead-free Electronics,* New Jersey, USA, Wiley.

Glazer, J. 1994. Microstructure and mechanical properties of Pb-free solder alloys for low-cost electronic assembly: A review. *Journal of Electronic Materials,* 23**,** 693-700.

Gong, J., Liu, C., Conway, P. P. & Silberschmidt, V. V. 2009. Initial formation of CuSn intermetallic compounds between molten SnAgCu solder and Cu substrate. *Scripta Materialia,* 60**,** 333-335.

Harrison, M., Vincent, J. & Steen, H. 2001. Lead-free reflow soldering for electronics assembly. *Soldering & surface mount technology,* 13**,** 21-38.

Haseeb, A. S. M. A., Arafat, M. M. & Johan, M. R. 2012. Stability of molybdenum nanoparticles in Sn–3.8Ag–0.7Cu solder during multiple reflow and their influence on interfacial intermetallic compounds. *Materials Characterization,* 64**,** 27-35.

Haseeb, A. S. M. A. & Leng, T. S. 2011. Effects of Co nanoparticle addition to Sn–3.8Ag–0.7Cu solder on interfacial structure after reflow and ageing. *Intermetallics,* 19**,** 707-712.

Ho, C., Lin, Y., Yang, S., Kao, C. & Jiang, D. 2006. Effects of limited Cu supply on soldering reactions between SnAgCu and Ni. *Journal of Electronic Materials,* 35**,** 1017-1024.

Humpston, G. & Jacobson, D. M. 2004. *Principles of Soldering*, USA, Asm International.

Hwang, C.-W., Lee, J.-G., Suganuma, K. & Mori, H. 2003. Interfacial microstructure between Sn-3Ag-xBi alloy and Cu substrate with or without electrolytic Ni plating. *Journal of Electronic Materials,* 32**,** 52-62.

Jianbiao, P., Tonkay, G. L., Storer, R. H., Sallade, R. M. & Leandri, D. J. 2004. Critical variables of solder paste stencil printing for micro-BGA and fine-pitch QFP. *Electronics Packaging Manufacturing, IEEE Transactions on,* 27**,** 125-132.

Kang, S. & Sarkhel, A. 1994. Lead (Pb)-free solders for electronic packaging. *Journal of Electronic Materials,* 23**,** 701-707.

Karakaya, I. & Thompson, W. T. 1987. The Ag-Sn (Silver-Tin) system. *Bulletin of Alloy Phase Diagrams,* 8**,** 340-347.

Koo, J.-M. & Jung, S.-B. 2005. Effect of substrate metallization on mechanical properties of Sn–3.5Ag BGA solder joints with multiple reflows. *Microelectronic Engineering,* 82**,** 569-574.

Korhonen, T., Su, P., Hong, S., Korhonen, M. & Li, C.-Y. 2000. Reactions of lead-free solders with CuNi metallizations. *Journal of Electronic Materials,* 29**,** 1194-1199.

Korhonen, T. M. & Kivilahti, J. K. 1998. Thermodynamics of the Sn-In-Ag solder system. *Journal of Electronic Materials,* 27**,** 149-158.

Kumar, A., Chen, Z., Mhaisalkar, S. G., Wong, C. C., Teo, P. S. & Kripesh, V. 2006. Effect of Ni–P thickness on solid-state interfacial reactions between Sn–3.5Ag solder and electroless Ni–P metallization on Cu substrate. *Thin Solid Films,* 504**,** 410-415.

Kumar, A., He, M. & Chen, Z. 2005. Barrier properties of thin Au/Ni–P under bump metallization for Sn–3.5Ag solder. *Surface and Coatings Technology,* 198**,** 283-286.

Kumar, K. M., Kripesh, V. & Tay, A. A. 2008. Single-wall carbon nanotube (SWCNT) functionalized Sn–Ag–Cu lead-free composite solders. *Journal of Alloys and Compounds,* 450**,** 229-237.

Laurila, T., Hurtig, J., Vuorinen, V. & Kivilahti, J. K. 2009. Effect of Ag, Fe, Au and Ni on the growth kinetics of Sn–Cu intermetallic compound layers. *Microelectronics Reliability,* 49**,** 242-247.

Laurila, T., Vuorinen, V. & Kivilahti, J. K. 2005. Interfacial reactions between lead-free solders and common base materials. *Materials Science and Engineering: R: Reports,* 49**,** 1-60.

Laurila, T., Vuorinen, V. & Paulasto-Kröckel, M. 2010. Impurity and alloying effects on interfacial reaction layers in Pb-free soldering. *Materials Science and Engineering: R: Reports,* 68**,** 1-38.

Lee, B.-J., Hwang, N. M. & Lee, H. M. 1997. Prediction of interface reaction products between Cu and various solder alloys by thermodynamic calculation. *Acta Materialia,* 45**,** 1867-1874.

Lee, K., Li, M. & Tu, K. 2003. Growth and ripening of (Au, Ni) Sn4 phase in Pb-free and Pb-containing solders on Ni/Au metallization. *Journal of Materials Research,* 18**,** 2562-2570.

Li, Y., Moon, K.-s. & Wong, C. 2005. Electronics without lead. *Science,* 308**,** 1419-1420.

Lin, C.-H., Chen, S.-W. & Wang, C.-H. 2002. Phase equilibria and solidification properties of Sn-Cu-Ni alloys. *Journal of Electronic Materials,* 31**,** 907-915.

Lin, K.-L. & Shih, P.-C. 2008. IMC formation on BGA package with Sn–Ag–Cu and Sn–Ag–Cu–Ni–Ge solder balls. *Journal of Alloys and Compounds,* 452**,** 291-297.

Liu, C. Y. & Tu, K. N. 1998. Morphology of wetting reactions of SnPb alloys on Cu as a function of alloy composition. *Journal of Materials Research,* 13**,** 37-44.

Liu, Y. C., Teo, J. W. R., Tung, S. K. & Lam, K. H. 2008. High-temperature creep and hardness of eutectic 80Au/20Sn solder. *Journal of Alloys and Compounds,* 448**,** 340-343.

M. Arden, W. 2002. The International Technology Roadmap for Semiconductors—Perspectives and challenges for the next 15 years. *Current Opinion in Solid State and Materials Science,* 6**,** 371-377.

Moon, K., Boettinger, W., Kattner, U., Biancaniello, F. & Handwerker, C. 2000. Experimental and thermodynamic assessment of Sn-Ag-Cu solder alloys. *Journal of Electronic Materials,* 29**,** 1122-1136.

Mordechay Schlesinger, P. D. 2010. *Modern Electroplating,*USA, John Wiley & Sons.

Müller, W. H. 2004. Morphology changes in solder joints—experimental evidence and physical understanding. *Microelectronics Reliability,* 44**,** 1901-1914.

Nai, S., Wei, J. & Gupta, M. 2006. Influence of ceramic reinforcements on the wettability and mechanical properties of novel lead-free solder composites. *Thin Solid Films,* 504**,** 401-404.

Oh, C.-S., Shim, J.-H., Lee, B.-J. & Dong Nyung, L. 1996. A thermodynamic study on the Ag ・ Sb ・ Sn system. *Journal of Alloys and Compounds,* 238**,** 155-166.

Okamoto, H. 2006. Ni−Sn (Nickel-Tin). *Journal of Phase Equilibria and Diffusion,* 27**,** 315-315.

Pang, J. H., Xu, L., Shi, X., Zhou, W. & Ngoh, S. 2004a. Intermetallic growth studies on Sn-Ag-Cu lead-free solder joints. *Journal of Electronic Materials,* 33**,** 1219-1226.

Pang, J. H. L., Low, T. H., Xiong, B. S., Luhua, X. & Neo, C. C. 2004b. Thermal cycling aging effects on Sn–Ag–Cu solder joint microstructure, IMC and strength. *Thin Solid Films,* 462–463**,** 370-375.

Park, J.-Y., Kabade, R., Kim, C.-U., Carper, T., Dunford, S. & Puligandla, V. 2003. Influence of Au addition on the phase equilibria of near-eutectic Sn-3.8 Ag-0.7 Cu Pb-free solder alloy. *Journal of Electronic Materials,* 32**,** 1474-1482.

Peng, W., Monlevade, E. & Marques, M. E. 2007. Effect of thermal aging on the interfacial structure of SnAgCu solder joints on Cu. *Microelectronics Reliability,* 47**,** 2161-2168.

Rizvi, M., Bailey, C., Chan, Y., Islam, M. & Lu, H. 2007. Effect of adding 0.3 wt% Ni into the Sn–0.7 wt% Cu solder: Part II. Growth of intermetallic layer with Cu during wetting and aging. *Journal of Alloys and Compounds,* 438**,** 122-128.

Schaefer, M., Fournelle, R. A. & Liang, J. 1998. Theory for intermetallic phase growth between Cu and liquid Sn-Pb solder based on grain boundary diffusion control. *Journal of Electronic Materials,* 27**,** 1167-1176.

Schoeller, H., Bansal, S., Knobloch, A., Shaddock, D. & Cho, J. 2009. Microstructure Evolution and the Constitutive Relations of High-Temperature Solders. *Journal of Electronic Materials,* 38**,** 802-809.

Shang, P. J., Liu, Z. Q., Pang, X. Y., Li, D. X. & Shang, J. K. 2009. Growth mechanisms of Cu3Sn on polycrystalline and single crystalline Cu substrates. *Acta Materialia,* 57**,** 4697-4706.

Shangguan, D. 2005. *Lead-Free Solder Interconnect Reliability,* USA, Asm International.

Sharif, A. & Chan, Y. C. 2005. Effect of indium addition in Sn-rich solder on the dissolution of Cu metallization. *Journal of Alloys and Compounds,* 390**,** 67-73.

Shen, J. & Chan, Y. C. 2009. Research advances in nano-composite solders. *Microelectronics Reliability,* 49**,** 223-234.

Shen, J., Liu, Y., Han, Y., Tian, Y. & Gao, H. 2006. RETRACTED: Strengthening effects of ZrO2 nanoparticles on the microstructure and microhardness of Sn–3.5 Ag lead-free solder. *Materials Science and Engineering: A,* 441**,** 135-141.

Shi, Y., Tian, J., Hao, H., Xia, Z., Lei, Y. & Guo, F. 2008. Effects of small amount addition of rare earth Er on microstructure and property of SnAgCu solder. *Journal of Alloys and Compounds,* 453**,** 180-184.

Sivasubramaniam, V., Bosco, N. S., Janczak-Rusch, J., Cugnoni, J. & Botsis, J. 2008. Interfacial Intermetallic Growth and Strength of Composite Lead-Free Solder Alloy Through Isothermal Aging. *Journal of Electronic Materials,* 37**,** 1598-1604.

Subramanian, P. R. & Laughlin, D. E. 1990. The Cu-Mo (Copper-Molybdenum) system. *Bulletin of Alloy Phase Diagrams,* 11**,** 169-172.

Suganuma, K. 2001. Advances in lead-free electronics soldering. *Current Opinion in Solid State and Materials Science,* 5**,** 55-64.

Suraski, D. & Seelig, K. 2001. The current status of lead-free solder alloys. *Electronics Packaging Manufacturing, IEEE Transactions on,* 24**,** 244-248.

Tai, F., Guo, F., Xia, Z., Lei, Y., Yan, Y., Liu, J. & Shi, Y. 2005. Processing and creep properties of Sn-Cu composite solders with small amounts of nanosized Ag reinforcement additions. *Journal of Electronic Materials,* 34**,** 1357-1362.

Takaku, Y., Felicia, L., Ohnuma, I., Kainuma, R. & Ishida, K. 2008. Interfacial Reaction Between Cu Substrates and Zn-Al Base High-Temperature Pb-Free Solders. *Journal of Electronic Materials,* 37**,** 314-323.

Tu, K. N. 2010. *Solder Joint Technology: Materials, Properties, and Reliability,* Springer.

Wang, H., Zhao, H., Sekulic, D. P. & Qian, Y. 2008a. A Comparative Study of Reactive Wetting of Lead and Lead-Free Solders on Cu and (Cu 6 Sn 5/Cu 3 Sn)/Cu Substrates. *Journal of Electronic Materials,* 37**,** 1640-1647.

Wang, J., Zhang, L. G., Liu, H. S., Liu, L. B. & Jin, Z. P. 2008b. Interfacial reaction between Sn–Ag alloys and Ni substrate. *Journal of Alloys and Compounds,* 455**,** 159-163.

Wang, Y., Lin, Y., Tu, C. & Kao, C. 2009. Effects of minor Fe, Co, and Ni additions on the reaction between SnAgCu solder and Cu. *Journal of Alloys and Compounds,* 478**,** 121-127.

Wild, R. 1971. Properties of some low melting fusible alloys. *IBM Federal Systems Division Laboratory Technical Report No,* 171200408.

Wilde, G. & Perepezko, J. 2000. Experimental study of particle incorporation during dendritic solidification. *Materials Science and Engineering: A,* 283**,** 25-37.

Wood, E. P. & Nimmo, K. L. 1994. In search of new lead-free electronic solders. *Journal of Electronic Materials,* 23**,** 709-713.

Wu, C. M. L., Yu, D. Q., Law, C. M. T. & Wang, L. 2004. Properties of lead-free solder alloys with rare earth element additions. *Materials Science and Engineering: R: Reports,* 44**,** 1-44.

Xie, Y. & Zhang, X. 1998. Phase diagram and thermodynamic properties of Ag−Cu alloys. *Science in China Series E: Technological Sciences,* 41**,** 348-356.

Yoon, J.-W., Noh, B.-I., Lee, Y.-H., Lee, H.-S. & Jung, S.-B. 2008. Effects of isothermal aging and temperature–humidity treatment of substrate on joint reliability of Sn–3.0Ag–0.5Cu/OSP-finished Cu CSP solder joint. *Microelectronics Reliability,* 48**,** 1864-1874.

Zakel, E., Azdasht, G. & Reichl, H. 1991. Investigations of laser soldered TAB inner lead contacts. *Components, Hybrids, and Manufacturing Technology, IEEE Transactions on,* 14**,** 672-679.

Zeng, G., Xue, S., Zhang, L., Gao, L., Dai, W. & Luo, J. 2010. A review on the interfacial intermetallic compounds between Sn–Ag–Cu based solders and substrates. *Journal of Materials Science: Materials in Electronics,* 21**,** 421-440.

Zerrer, P., Fix, A., Hutter, M. & Pape, U. Year. NanoFlux—doping of solder pastes. *In:* Electronics System-Integration Technology Conference, 2008. ESTC 2008. 2nd, 2008. IEEE, 923-928.

Zhang, L., Xue, S., Chen, Y., Han, Z., Wang, J., Yu, S. & Lu, F. 2009. Effects of cerium on Sn-Ag-Cu alloys based on finite element simulation and experiments. *Journal of Rare Earths,* 27**,** 138-144.

Zribi, A., Clark, A., Zavalij, L., Borgesen, P. & Cotts, E. 2001. The growth of intermetallic compounds at Sn-Ag-Cu solder/Cu and Sn-Ag-Cu solder/Ni interfaces and the associated evolution of the solder microstructure. *Journal of Electronic Materials,* 30**,** 1157-1164.